Case Studies in Construction Materials 24 (2026) e05929

Contents lists available at ScienceDirect

Case Studies in Construction Materials

journal homepage: www.elsevier.com/locate/cscm

Long-term stiffness trends of concrete beams with carbon fiber and steel reinforcement: Experimental and analytical evaluation after retrofitting, repeated loading, and environmental exposure

Haji Akbar Sultani, Violetta K. Kytinou, Aleksandr Sokolov, Viktor Gribniak *

Laboratory of Innovative Building Structures, Vilnius Gediminas Technical University, Saulėtekio av. 11, Vilnius LT-10223, Lithuania

ARTICLE INFO

Keywords:
Reinforced concrete
Composite reinforcement systems
Bending test
Analytical model
Residual stiffness
Repeated mechanical loading
Environmental exposure
Long-term durability assessment

ABSTRACT

The durability of composite reinforcement systems under combined mechanical and environmental actions remains insufficiently documented. Most studies rely on qualitative comparisons or ultimate strength, leaving a gap in quantifying the evolution of stiffness under service loads—a key parameter for long-term reliability. This study evaluates residual flexural stiffness of composite reinforcement systems—including externally bonded reinforcement (EBR), near-surface-mounted (NSM) strips, and hybrid configurations combining unidirectional carbon fiber (CF) reinforcement and steel bars—under repeated mechanical loading and long-term environmental exposure. The program included 26 beams, seven of which were retrofitted with CF sheets or strips after prior bending tests to simulate rehabilitation scenarios. These retrofitted cases revealed a critical limitation of the analytical approach: evaluating stiffness requires correcting for residual curvature in previously damaged bending samples. The experimental program spanned up to three years under open-air conditions. This study demonstrates the applicability of the equivalent tensile-stress measure of flexural stiffness under natural long-term exposure, extends and formalizes a previously validated analytical framework originally applied under short-term conditions, and provides practical guidance for further tests. The results confirm that NSM systems outperform EBR alternatives in long-term durability. Quantitatively, the NSM systems maintained nearly constant residual stiffness, whereas the EBR systems exhibited approximately a 20 % reduction under outdoor exposure relative to laboratory-stored specimens. In contrast, hybrid systems showed a synergistic mechanical response, reducing vulnerability to environmental degradation even when retrofitted after steel yielding. The proposed methodology quantifies the effects of reinforcement material interaction in laboratory-scale elements and is not intended for direct structural-design verification. The findings represent general tendencies that motivate future long-term investigations and contribute to durability-based materials engineering applicable under realistic service conditions.

1. Introduction

Composite reinforcement systems have become increasingly prominent in structural engineering due to their high strength-to-weight ratio, corrosion resistance, and adaptability to various strengthening scenarios [1–3]. Among these systems, carbon

* Corresponding author.
E-mail address: viktor.gribniak@vilniustech.lt (V. Gribniak).

https://doi.org/10.1016/j.cscm.2026.e05929
Received 1 December 2025; Received in revised form 9 January 2026; Accepted 20 February 2026
Available online 22 February 2026
2214-5095/© 2026 The Author(s). Published by Elsevier Ltd. This is an open access article under the CC BY license (http://creativecommons.org/licenses/by/4.0/).

fiber-reinforced polymer (CFRP) materials are widely used in externally bonded reinforcement (EBR) and near-surface-mounted (NSM) configurations to enhance the flexural performance of reinforced concrete (RC) elements [4–7]. Glass fiber-reinforced polymer (GFRP) bars also offer corrosion resistance [8–10] and are often embedded as internal reinforcement in new or rehabilitated structures. However, despite their widespread application, concerns remain regarding their long-term performance under combined mechanical and environmental actions [11–14].

While short-term performance metrics—such as ultimate load capacity and initial stiffness—are well documented, the degradation of mechanical properties over extended periods has not been sufficiently quantified. This limitation is especially pronounced for reinforcement systems exposed to open-air environments, where factors such as moisture ingress, temperature fluctuations, and ultraviolet (UV) radiation can significantly affect bond integrity and material behavior [4,15–19]. Moreover, most available studies rely on qualitative comparisons or simplified assumptions, lacking a scalable, physically interpretable measure to quantify stiffness changes and compare reinforcement strategies [20–24].

1.1. Background, gaps, and scope

The long-term mechanical performance of composite reinforcement systems remains insufficiently documented despite their increasing use in structural strengthening and rehabilitation applications. Existing studies on CFRP-based systems—whether EBR sheets [4–7], NSM strips [25,26], or internal GFRP bars [8–10]—have predominantly focused on ultimate capacity, bond behavior, and short-term mechanical response. However, these parameters provide only a partial perspective on durability, as reinforcement systems in service rarely fail by reaching ultimate strength; instead, they experience progressive stiffness degradation governed by bond deterioration, adhesive aging, concrete microcracking, and environmental stressors such as moisture ingress, UV exposure, thermal cycling, and freeze-thaw actions [4,6,16,17,19,27–29]. Recent publications [6,16,18,27] have emphasized bond durability, environmental aging mechanisms, and local failure modes, but quantitative evaluation of stiffness evolution under service load remains limited [30–32].

Investigations addressing hygrothermal degradation [18,27], chloride exposure [4], surface-treatment effects [6], or high-temperature behavior [17] typically report bond strength or ultimate capacity losses rather than service-load stiffness changes. Consequently, the literature lacks a unified, physically interpretable indicator capable of quantifying stiffness degradation in a reproducible manner across reinforcement types, exposure conditions, and load histories. This gap is particularly evident for systems incorporating CFRP sheets or strips, where the adhesive layer directly governs composite efficiency and is highly susceptible to environmental effects.

To address these limitations, the present investigation adopts an analytical framework that expresses residual flexural stiffness through equivalent tensile stress in concrete [14,17,20,33], enabling direct comparison across reinforcement strategies (EBR, NSM, and hybrid systems) and storage conditions (laboratory vs. outdoor). This framework complements the broader durability literature [18,19,26] by shifting the focus from ultimate-state behavior to service-load performance, which is more relevant for structural reliability and long-term serviceability [34–37].

The investigation analyzes laboratory-scale beams purposely designed to form multiple cracks in the pure bending zone and to maintain a near-rectangular approximation of tensile stresses, thereby isolating material-interaction effects between reinforcement and concrete [14,17,20,33]. The methodology targets service-load behavior and composite interaction rather than discrete crack modeling or code-level design verification. This framing anticipates potential misaligned expectations and clearly states the applicability boundaries under natural exposure conditions, where NSM systems may demonstrate improved stability relative to EBR [4,25,26]. At the same time, environmental stressors (moisture, UV/thermal cycling, freeze-thaw) govern the attenuation of stiffness [4,6,16,17,19,27–29].

1.2. Relation to previous work

Sultani et al. [33] introduced a residual stiffness analysis procedure that combined slab-shaped bending samples—designed to ensure multiple cracks in a short pure-bending zone of relatively small (laboratory-scale) elements—with a near-rectangular distribution of stresses in the tensile concrete. The corresponding analytical model provided an explicit solution to the residual stiffness problem, expressed in terms of the equivalent tensile stresses acting in the tension concrete. This explicit solution ensured precision equivalent to that of the measurement devices and remained independent of the loading protocol (including cyclic and repeated loads) and reinforcement arrangement (including hybrid systems). Gribniak et al. [20] systematized this analysis layout, formulated the concept of “standardized” testing, and optimized the procedure for estimating equivalent stresses.

The study by Sultani et al. [38] represents the first attempt to apply the standardized testing concept to quantify adverse environmental effects on the mechanical performance of composite reinforcement systems. However, this investigation did not account for residual (permanent) deformations after mechanical loading, which limited the interpretation of long-term changes in stiffness. Sultani et al. [14] further extended the methodology to repeated loading conditions, highlighting the fundamental necessity of capturing residual curvature to correctly interpret test results when bending elements undergo complete unloading between repetitions. This study also identified the vulnerability of glass-fiber reinforced polymer (GFRP) bars to repeated cyclic loads, emphasizing the need for reliable anchorage when such bars are used in cyclic environments.

Gribniak et al. [17] applied the analysis approach to evaluate the effects of elevated temperature (60 °C) in combination with repeated mechanical loading on the performance of carbon-fiber EBR systems. Because the specimens were transferred to a heating chamber between mechanical repetitions, the study adopted a residual-curvature accumulation approach to reposition

load-displacement diagrams and thus maintain a consistent stiffness measure. The results demonstrated a gradual decrease in equivalent tensile stress after the third heating repetition, with composite action disappearing after approximately five repetitions. Microstructural observations attributed this decline to the degradation of the adhesive layer that bonds the CFRP sheet to the concrete surface. Notably, the study confirmed the methodology's scalability by reducing specimen dimensions to 150 × 75 × 600 mm, thereby demonstrating applicability under equipment-limited testing conditions (e.g., heating-chamber constraints).

The recent publication by Gribniak et al. [39] extended the residual-stiffness concept to heat-resistant concretes. Using both bending and pull-out tests, the authors showed that ribbed stainless-steel bars in a modified castable mixture can maintain composite interaction at elevated temperatures. Bending-test results demonstrated composite action up to 600 °C.

Taken together, these prior studies define the analytical and experimental foundations of the present work. They justify the continued use of EBR and NSM configurations—both of which represent practical strengthening systems where composite interaction is highly sensitive to environmental exposure—and motivate the use of laboratory-scale elements whose geometry ensures multiple cracks with narrow spacing. Still, they provide an indispensable platform for isolating and comparing composite-interaction effects across reinforcement systems under service-load conditions.

Fig. 1 summarizes these methodological developments, illustrating how standardized equivalent-stress quantification [20,33] evolved through environmental exposure studies [38], through the explicit accounting of residual curvature [14,17], and through material-domain extensions [39]. The present study builds upon this progression by applying the standardized indicator under long-term natural exposure and formalizing the interpretation procedure for retrofitted elements, where prior damage and residual curvature critically influence stiffness estimation. The proposed methodology focuses on the material-interaction behavior of composite reinforcement systems. It remains applicable to structural analysis only with substantial reservations, given the specific geometry of the laboratory-scale specimens and the simplifying assumptions of the analytical model discussed in **Section 3**.

1.3. Objectives and contribution of the present study

The present study investigates the long-term residual flexural stiffness of composite reinforcement systems—externally bonded (EBR), near-surface-mounted (NSM), and hybrid steel-CFRP configurations—under repeated mechanical loading and natural multi-year environmental exposure. The analytical evaluation employs the equivalent tensile stress indicator, enabling a consistent comparison of the evolution of stiffness at a predefined service-load level. A specific objective is to clarify the influence of residual

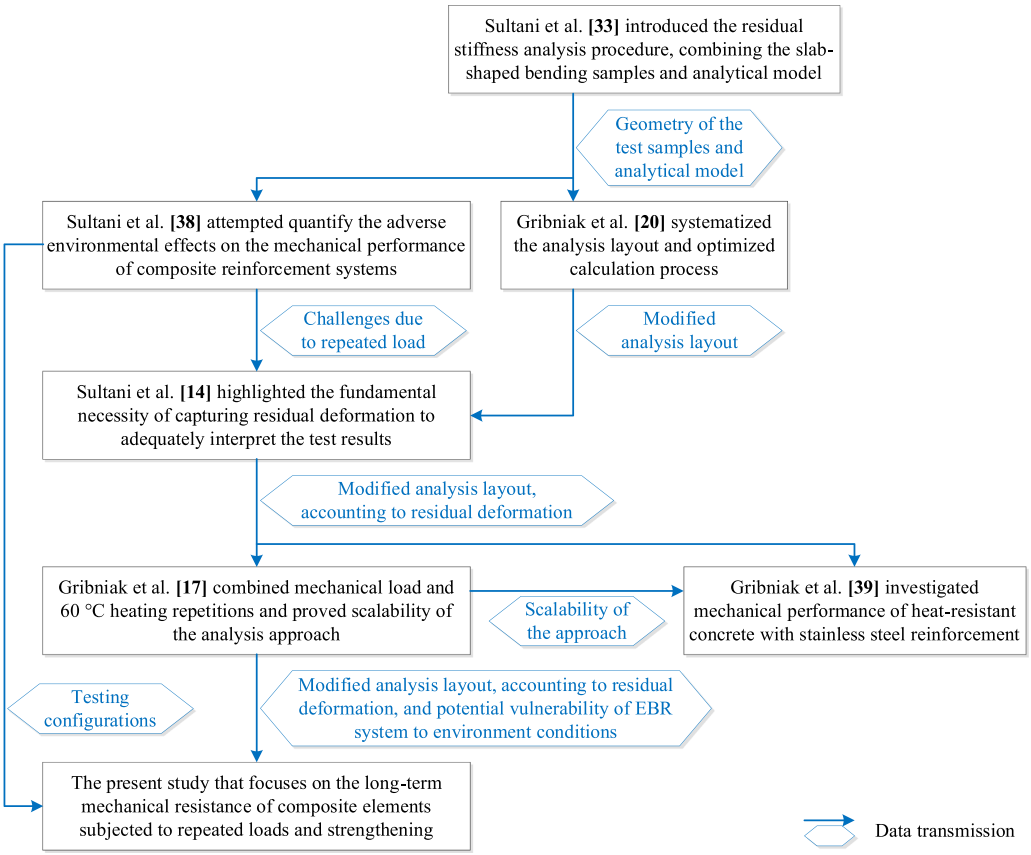


Fig. 1. Relationship between the previous publications [14,17,20,33,38,39] and the present study.

curvature in retrofitted specimens, where prior mechanical damage may artificially amplify stiffness unless explicitly corrected. The study establishes a coherent framework for interpreting stiffness degradation in composite reinforcement systems subjected to realistic service scenarios.

This study contributes to materials engineering and composite-reinforcement science by demonstrating, for the first time, the applicability of the equivalent tensile-stress measure of flexural stiffness under natural long-term exposure, thereby expanding and formalizing a previously validated short-term methodology. The investigation establishes a physically interpretable, reproducible measure of stiffness degradation for CFRP-based reinforcement systems, grounded in material-interaction mechanisms rather than purely structural metrics. The study compares the long-term stiffness tendencies of EBR, NSM, and hybrid steel-CFRP systems within a unified evaluation framework. The study provides a material-oriented, durability-focused perspective that informs the development of composite reinforcement systems resilient to environmental effects and supports future standardization of stiffness-based performance evaluation.

Table 1
Geometry and mechanical characteristics of the beam samples.

Nr.	Beam	h	b	d_1	d_2	d_r	A_1	A_2	A_r	E_1	E_2	$n\rho$	f_c		Testing age◊
		[mm]					[mm^2]			[GPa]		[%]	[MPa]		[days]
1.	S1L	106	197	89	–	89	100.5	–	100.5	202	–	3.26	44.2 ± 0.89		13
2.	S2L	106	200	79	–	79	84.82	–	84.82	195	–	3.77	21.8 ± 0.85		33
3.	S3L-1	103	200	79	–	79	150.8	–	150.8	195	–	6.88	21.8 ± 0.85		33
4.	S3L-2	103	200	79	–	79	150.8	–	150.8	195	–	5.40	46.0 ± 1.59		33
5.	EL-1	102	199	–	103	103	–	32.8	32.8	–	230	1.03	50.7 ± 1.53		48
6.	EL-2	103	199	–	104	104	–	32.8	32.8	–	230	1.02	50.7 ± 1.53		47
7.	EL-3	104	198	105	–	105	–	32.8	32.8	–	230	1.03	54.8 ± 0.41	59.8 ± 0.89‡	119/274/1093
8.	EL-4	105	197	106	–	106	–	32.8	32.8	–	230	0.96	54.7 ± 0.99	59.8 ± 0.89‡	116/271/1090
9.	NL-1	104	200	–	94	94	–	28.0	28.0	–	170	0.72	49.6 ± 2.58		62
10.	NL-2	105	197	–	95	95	–	28.0	28.0	–	170	0.71	50.7 ± 2.51		63
11.	NL-3	103	199	93	–	93	–	28.0	93.0	–	170	0.73	54.8 ± 0.41	60.1 ± 0.89‡	120/274/1442
12.	NL-4	104	198	94	–	94	–	28.0	28.0	–	170	0.73	54.8 ± 0.41	60.1 ± 0.89‡	119/274/1442
13.	NSL-1	108	197	77	92	83	38.1	28.0	61.2	206	170	2.30	34.1 ± 2.92		14
14.	NSL-2*	101	200	67	– 92	67 76	38.1	– 28.0	38.1 61.2	206	– 170	1.83 2.59	35.2 ± 3.05		26
15.	E-1	105	201	106	–	106	–	32.8	32.8	–	230	1.01	54.8 ± 0.41	72.7 ± 1.89‡	119/274/1093
16.	E-2	104	198	105	–	105	–	32.8	32.8	–	230	1.02	54.8 ± 0.41	72.7 ± 1.89‡	119/276/1093
17.	E-3	106	197	106	–	106	–	32.8	32.8	–	230	1.02	54.8 ± 0.41	72.7 ± 1.89‡	119/273/1093
18.	N-1	103	200	93	–	93	–	28	28.0	–	170	0.65	68.7 ± 0.99	86.1 ± 1.97‡	116/273/1440
19.	N-2	102	200	92	–	92	–	28	28.0	–	170	0.66	68.7 ± 0.99	86.1 ± 1.97‡	117/270/1439
20.	N-3	100	201	90	–	90	–	28	28.0	–	170	0.67	68.7 ± 0.99	86.1 ± 1.97‡	116/270/1439
21.	ES1-1*	104	197	90	– 106	90 94	100.5	– 32.8	100.5 126.9	206	– 230	3.38 4.41	44.8 ± 1.38	80.1 ± 3.00‡	14 35/189/1358
22.	ES1-2*	104	199	91	– 106	91 95	100.5	– 32.8	100.5 126.9	206	– 230	3.31 4.33	44.8 ± 1.38	80.1 ± 3.00‡	14 35/190/1358
23.	ES2-1*	108	200	82	– 109	82 90	83.22	– 32.8	83.22 111.2	202	– 230	3.04 4.00	41.5 ± 1.64	–†	43 877/914/1067/2235
24.	ES2-2*	104	200	79	– 105	79 87	83.22	– 32.8	83.22 111.2	202	– 230	3.08 4.05	45.0 ± 1.41	–†	57 877/914/1067/2235
25.	ES3-1*	105	200	77	– 106	77 83	149.8	– 32.8	149.8 177.2	205	– 230	5.57 6.46	50.6 ± 3.01	–†	43 877/914/1067/2236
26.	ES3-2*	105	200	79	– 106	79 84	149.8	– 32.8	149.8 177.2	205	– 230	5.76 6.73	41.5 ± 1.41	–†	38 878/913/1067/2236

*The steel-reinforced beams strengthened with CFRP after the mechanical load; ‡Correspond to the last testing day; †Additional cylinders were not produced to determine the concrete strength at the last testing day. ◊A single number indicates the testing age; multiple numbers denote the age at successive testing stages: first loading repetition / second loading repetition / … / final testing.

2. Experimental program

The experimental program was designed to investigate the long-term mechanical performance of composite reinforcement systems under realistic service conditions, including repeated mechanical loading and environmental exposure. Recognizing the multifaceted nature of durability in RC structures, the study integrates several layers of complexity: different reinforcement configurations (embedded bars, EBR, NSM, hybrid systems), varied loading protocols (pseudo-monotonic, repeated, and cyclic), and distinct environmental conditions (laboratory-stored versus open-environment exposed specimens). This structured approach enables an explicit evaluation of residual stiffness and degradation mechanisms across reinforcement strategies. **Sections 2.1** to **2.3** detail the specimen design, material properties, and strengthening configurations, while **Sections 2.4** to **2.6** describe the loading protocols, environmental exposure setup, and long-term testing procedures.

2.1. Overview of the test program

The experimental program aimed to evaluate long-term residual stiffness of composite reinforcement systems under repeated loading and environmental exposure through a multi-phase testing approach. The program includes several distinct specimen groups and loading protocols, each selected to illustrate specific aspects of the analytical methodology [14,17,33]. Pseudo-monotonic bending tests were first conducted to determine the load-bearing capacity of the specimens, enabling the definition of service load levels for subsequent stiffness degradation analysis. Repeated mechanical loading tests—where the load was entirely removed after each cycle—were performed to isolate the effect of mechanical fatigue on residual stiffness.

In addition to primary reinforcement configurations, the program includes specimens strengthened with CFRP materials following prior mechanical testing of steel-reinforced elements. These cases simulate realistic rehabilitation scenarios and highlight the challenges of interpreting residual stiffness when prior deformation must be accounted for. To address this challenge, the methodology incorporates residual curvature-based correction to ensure accurate positioning of the response diagrams and to avoid artificially stiff analytical outcomes.

Finally, long-term tests lasting up to three years were conducted on selected reinforcement systems—specifically those identified as potentially vulnerable to environmental degradation [17] . Previous findings [14,17,33] substantiated the selection, and the long-term exposure conditions were designed to replicate realistic service environments. Together, these test phases provide a comprehensive dataset for validating the analytical framework and quantifying the durability of composite reinforcement systems.

The specimen designations, reinforcement types, and loading protocols are summarized in Table 1, which provides a structured overview of the test matrix. In this table, h and b define the height and width of the cross-section; d_1, d_2, and d_r are the effective depth of the reinforcement components “1” and “2,” and the transformed depth value; A_1, A_2, and A_r are the cross-section area of the reinforcement components “1” and “2,” and the transformed area; E_1 and E_2 are the modulus of elasticity of the reinforcement components “1” and “2;” $n\rho$ is the product of the modular ratio of the reinforcement and concrete and the reinforcement ratio as described in [20] ; f'_c is the compressive strength of the ∅150 × 300 mm concrete cylinders on the first and last testing days.

The following equation determines the transformed parameters of the reinforcement in Table 1:

$$d_r = \frac{\sum_{i=1}^{2} E_i A_i d_i}{\sum_{i=1}^{2} E_i A_i}, \quad A_r = \frac{1}{E_1} \sum_{i=1}^{2} E_i A_i \,. \tag{1}$$

This equation assumes the modulus of elasticity of steel reinforcement (E_1) as a reference. These transformed parameters are directly employed in the analytical evaluation (**Section 3**), where they enter the equilibrium formulation and define the stiffness indicator expressed through equivalent tensile stress.

In Table 1, the compressive strength of the concrete (f'_c) was determined from the ∅150 × 300 mm cylinders on the first and last testing days of the beam specimens. The last column of Table 1 shows specimen age at each testing stage; slashes separate ages for repeated loading tests. The f'_c values represent the average and standard deviation obtained from three identical cylinders. The remaining concrete parameters required for the analytical model—namely, the modulus of elasticity and tensile strength—were derived from the average compressive strength using *Eurocode 2* formulas [40] , as validated by Gribniak et al. [41,42] for numerical modeling of reinforced concrete elements.

The second column of Table 1 lists the tested beam specimens using a structured notation system. The letter N denotes beams reinforced with NSM CFRP strips, while E refers to specimens strengthened using EBR CFRP sheets. The letter L indicates that the specimens were stored under laboratory conditions, and the accompanying number identifies identical specimens within each group. The letter S corresponds to beams with steel reinforcement, specifically: three 5 mm bars (S), two 8 mm bars (S1), three 6 mm bars (S2), and three 8 mm bars (S3). The combination ES denotes a hybrid reinforcement system integrating EBR CFRP sheets and steel bars. Notably, specimens #14 and #21 to #26 were initially tested with steel reinforcement and subsequently strengthened with CFRP materials.

2.2. Materials and specimen design

The experimental program involved several groups of RC specimens. All test specimens were cast using structural-grade concrete

with a target compressive strength of about 40 MPa. The beam samples were created in multiple batches using the same concrete proportions. For one cubic meter, the concrete mixture included: 356 kg of cement CEM I 42.5 R, 177 kg of limestone powder, 163 liters of water, 890 kg of 0/4 mm sand, and 801 kg of 4/16 mm crushed granite aggregates; 7.0 kg of superplasticizer Mapei Dynamon XTend (Mapei AS, Sagstua, Norway), and 3.5 kg of the admixture SCP 1000 Optimizer (Spray-Lock Concrete Protection LLC, Chattanooga, TN, USA). The mixture also included 5.1 kg of Durus EasyFinish synthetic macro-fibers and Crackstop M Ultra micro-fibers (Adfil NV, Ghent, Belgium), mixed at a 4.67:1 ratio, to reduce the risk of brittle failure in the bending samples. Gribniak et al. [20] proved the effectiveness of this solution in enhancing concrete ductility.

Beam specimens, 1000 mm in length and rectangular 100 × 200 mm cross-section, were designed for four-point bending tests, which underlie the simplified stiffness quantification procedure described in **Section 3**. In particular, the extended cross-section width ensures that the rectangular stress distribution in the tensile concrete zone remains valid, which underlies the simplified stiffness quantification procedure. This slab-like shape promotes the formation of multiple cracks in the pure bending zone, enabling the application of the smeared crack model and supporting the assumption of a uniform tensile stress distribution, as mentioned in **Section 1.2**.

All beam samples were cast using steel forms and demolded 2–3 days after pouring. The specimens were cured at an average relative humidity of 73 % and a temperature of 20 °C before testing or forming the EBR and NSM systems. Six ∅150 × 300 mm cylinders were produced in each fabrication batch to determine the concrete's compressive strength, as reported in Table 1. The reinforcement systems varied across the specimen groups. They included EBR carbon fiber (CF) sheets, NSM CFRP strips, hybrid configurations combining steel and CFRP reinforcement, and retrofitted systems where CFRP materials were applied to previously tested steel-reinforced specimens. These configurations were selected to reflect practical strengthening scenarios and to enable comparative analysis under identical loading and environmental conditions. Fig. 2**a** shows the surface appearance of the reinforcement materials. The reinforcement layouts are illustrated in Fig. 2**b**, which shows the positions of EBR CF sheets and NSM strips relative to the concrete cross-section. Fig. 2**b** also includes hybrid reinforcement configurations that investigate the interaction between steel bars and CFRP components.

Table 2 specifies the mechanical properties and cross-section geometry of the reinforcement materials used in this study. The ribbed bars were made from the S500 structural steel. All fiber-based materials were commercially available unidirectional CF sheets and CFRP strips. In this study, CF denotes unidirectional carbon fiber sheets used in EBR systems, while CFRP denotes pultruded composite strips used in NSM configurations. Both belong to the family of carbon fiber-reinforced polymers but differ in geometry and installation technique.

The EBR system was formed using MapeWrap C UNI-AX CF sheets by Mapei S.p.A. (Italy). The NSM system employed unidirectional CFRP strips (S&P Clever Reinforcement Company AG, Switzerland). The mechanical properties and cross-sectional parameters of the CFRP reinforcement systems (i.e., EBR and NSM) were provided by the manufacturers. In contrast, the tensile characteristics of the steel reinforcement listed in Table 2 were determined by Rimkus and Gribniak [43] by testing three identical steel bar samples.

2.3. Reinforcement configurations and strengthening strategies

The experimental program included a diverse set of reinforcement configurations to reflect both conventional and advanced strengthening strategies used in structural engineering practice. The primary focus was placed on composite reinforcement systems applied in EBR and NSM configurations. In addition, the study incorporated hybrid systems combining unidirectional CF-materials (sheets and strips) with internal steel reinforcement. Including these configurations enabled direct comparison under identical

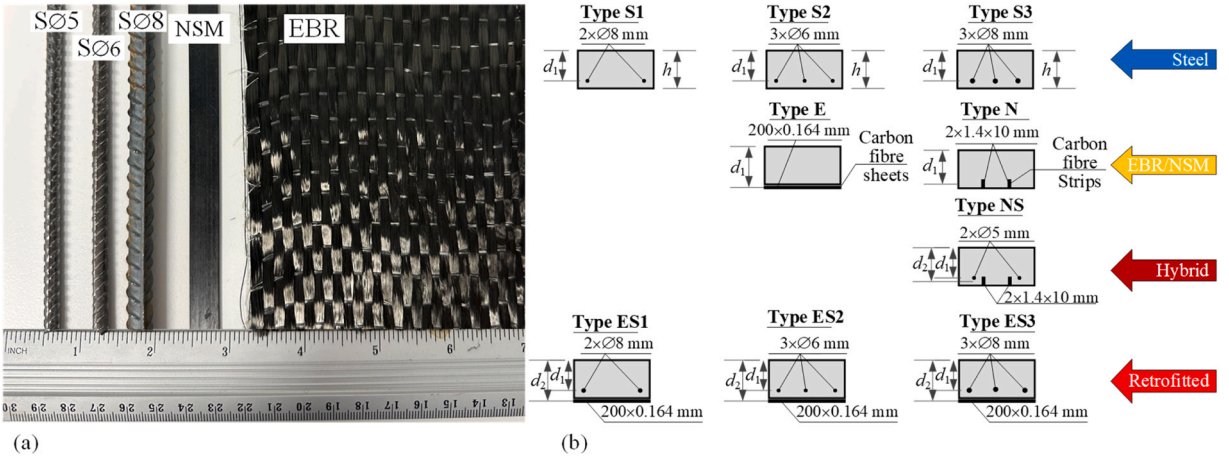


Fig. 2. Reinforcement characteristics: (a) the surface treatment of the reinforcement materials; (b) cross-sections of the beam samples. **Note:** EBR = externally bonded reinforcement (carbon fiber-reinforced sheet); NSM = near-surface mounted (unidirectional carbon fiber reinforced polymer strip); S = steel bars.

Table 2
Mechanical properties and geometry of the reinforcement materials.

Material type	Cross-section [mm]	Modulus of elasticity, E [GPa]	Yield strength, f_y [MPa]	Ultimate strength, f_u [MPa]	Elongation at break, ε_u [%]
CF EBR	100 × 0.164	230	–	4900	> 2
CFRP NSM	10 × 1.4	170	–	2800	> 16
Steel bars	⌀5	205 ± 3.4	566.4 ± 19.63	656.8 ± 3.57	3.8 ± 0.30
	⌀6	202 ± 2.8	468.3 ± 13.69	629.6 ± 5.90	6.2 ± 0.97
	⌀8	205 ± 18.3	483.9 ± 17.23	610.4 ± 33.10	13.9 ± 2.97

loading and environmental conditions. The reference hybrid NSL-1 beam sample combined NSM CFRP reinforcement with embedded steel reinforcement before the mechanical tests. The remaining hybrid systems (marked in Table 1 with asterisks) were retrofitted with CF EBR sheets after mechanical testing of RC beams reinforced with steel bars. The post-test strengthening was performed using either EBR or NSM techniques, depending on the specimen group. This approach enabled evaluation of residual stiffness in retrofitted elements and the effectiveness of CF-materials in restoring, or even enhancing, structural performance after prior mechanical loading-induced cracking. Table 1 summarizes the reinforcement characteristics, including cross-sectional areas, effective depths, and material properties.

The EBR systems employed unidirectional CF sheets bonded to the tension face of the concrete beams using a two-component epoxy adhesive. Before bonding, the concrete surface was cleaned, leveled with epoxy putty, and primed to ensure uniform adhesion. The installation procedure employs the wet layup technology [44] , including surface preparation, application of MapeWrap Primer 1 and MapeWrap 11/12 for leveling, impregnation of fibers with MapeWrap 21, and manual placement of the CF sheets. These sheets were cured under ambient conditions for seven days before testing. Fig. 3**a** shows the beam surfaces prepared for attachment of the CF sheets. The same procedure was consistently applied to all beam specimens strengthened using the EBR method after mechanical tests (i.e., elements #21–#26 in Table 1). Fig. 3**b** shows the EBR specimens after the CF sheets were attached.

The NSM systems consisted of pultruded CFRP strips embedded in pre-cut grooves along the beam specimens' tension surface, as shown in Fig. 3**c**. The grooves were filled with a two-component epoxy adhesive (S&P Resin 220, S&P Clever Reinforcement Company AG, Switzerland), and the strips were manually installed (pressed) into place and leveled to ensure uniform bonding. This procedure followed the manufacturer's recommendations [45] . The adhesive was allowed to cure for seven days before testing. Fig. 3**d** shows the NSM beam specimens after the CFRP strips were tightly embedded in the epoxy to eliminate voids and achieve uniform bonding. The same procedure was used to strengthen the sample NSL-2 after the mechanical test.



Fig. 3. Composite reinforcement systems: (a) specimens prepared for attaching EBR sheets; (b) formed EBR systems; (c) specimens with grooves for installing CFRP strips; (d) specimens with NSM CFRP strips. **Note:** The beams are shown inverted to clarify the installation details.

2.4. Test Setup and Loading Protocol

The mechanical testing of the specimens was conducted using a four-point bending configuration, which ensures a constant moment region and facilitates the evaluation of flexural stiffness degradation. The loading scheme and test setup are shown in Fig. 4.

The deformations in the pure bending zone were captured using linear variable-displacement transducers (LVDTs) and two digital image correlation (DIC) systems. Nine LVDTs distributed beneath the beam sample, as shown in Fig. 4**a**, measured the vertical displacements. Two single-lens reflex EOS 77D SLR cameras (Canon Inc., Tokyo, Japan), with an 18–135 mm EF-S lens (Canon Inc., Tokyo, Japan) and a remote control (ensuring the image stability), were positioned 0.5 m from the opposite sides of the bending zone, as shown in Fig. 4**b**. The cameras' settings were as follows: 1/200 s exposure, f/4.5 aperture, 24 mm focal length, and ISO 100. The DIC systems monitored surface deformations and cracking patterns. The GOM Correlate software (GOM Metrology, Germany) tracked pixel movements and mapped strain distributions.

The average curvature in the pure bending zone was used to separate the flexural response from shear effects, as required by the analytical model. Therefore, the further theoretical explanations also consider the moment-curvature behavior of the bending zone. The developed testing procedure (Fig. 4) estimates curvature in two ways: using vertical displacement and side-surface deformation results. The following formula relates the vertical displacement readings and the average curvature (κ):

$$\kappa = \frac{8 \bullet \Delta}{l^2 + 4 \bullet \Delta^2}; \quad \Delta = \frac{1}{3}\left(\sum_{i=4}^{6}\delta_i - \sum_{i=1}^{3}\delta_i - \sum_{i=7}^{9}\delta_i\right), \tag{2}$$

where Δ is the deflection of the bending zone of length $l = 600$ mm; δ_i is the vertical displacement captured by the i-th LVDT (L_i, see Fig. 4**a**).

As Fig. 4**a** shows, the surface deformations (relative displacement of pixels) were captured along the "top" and "bottom" lines at four points. The following equation relates the average curvature and the surface deformation results obtained by the DIC systems:

$$\kappa = \frac{\sum \upsilon}{d_u}; \quad \sum \upsilon = \frac{1}{3 \bullet l_u}\left(\sum_{i=1}^{3} u_i^t + \sum_{i=1}^{3} u_i^b\right), \tag{3}$$

where $\sum \upsilon$ is the total strain of the side surface; u_i^t and u_i^b are the relative displacements over the "top" and "bottom" DIC bases; l_u and d_u are the length of the monitoring bases (200 mm) and the distance between these lines (55 mm). The symmetrical distribution of digital cameras on both sides of the beam sample ensures two equivalent sets of deformations for estimating curvature. Previous studies [14,17,20,42] demonstrated the robustness of vertical displacement for estimating average curvature. Therefore, the present study also considers the vertical displacement and Eq. 2, the primary measure of the average curvature of the pure bending zone, employing DIC measurements (Eq. 3) only for verification.

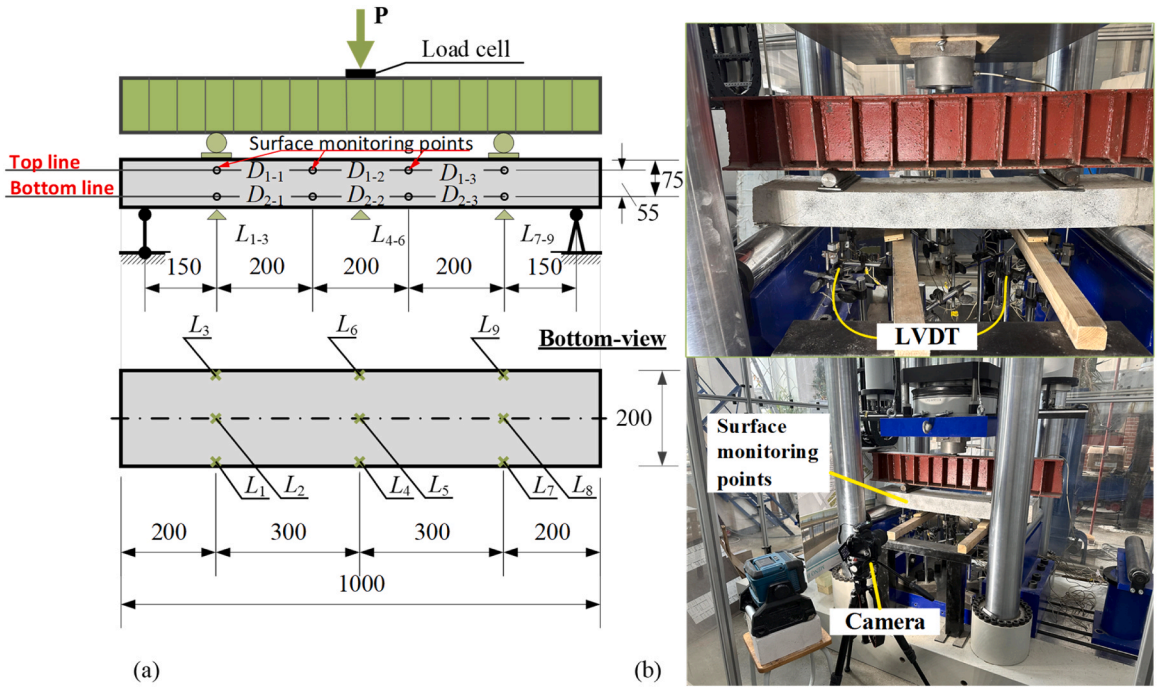


Fig. 4. Testing procedure: (a) loading and measurement scheme; (b) test setup and the DIC system.

The loading protocol was designed to mimic service conditions. A representative specimen from each group—except NSL-type samples—was tested under pseudo-monotonic bending to determine its load-bearing capacity ($\mathbf{M}_{ult}$). The load was applied at a steady displacement rate of 0.4 mm/min using a servo-hydraulic testing machine (Walter + Bai AG, Löhningen, Switzerland), with load control and data collection managed by Dion 7 software (Walter + Bai AG, Löhningen, Switzerland). Based on these results, a service load level ($\mathbf{M}_{ser}$) was set at approximately 55 % of the ultimate moment capacity, consistent with the design principles for RC bending samples [41,42]. To isolate the effects of mechanical fatigue, repeated loading tests were conducted in stages. Each stage involved five load cycles oscillating ±15 % around the target service moment. The load cycles were generated semi-automatically at a displacement rate of 0.4 mm/min, the same as in the monotonic tests, up to the maximum cycle boundary $\mathbf{M}_{max}$, and manually reduced to the minimum cycle boundary $\mathbf{M}_{min}$. For specimens with hybrid reinforcement, the loading protocol was adjusted to account for both steel and CFRP components, ensuring the applied moment stayed within the elastic range of the steel reinforcement.

Table 3 summarizes the loading parameters for each specimen group, including the minimum ($\mathbf{M}_{min}$), maximum ($\mathbf{M}_{max}$), service ($\mathbf{M}_{ser}$), and ultimate ($\mathbf{M}_{ult}$) moments. The loading protocol "M" was used to determine the load-bearing capacity of the reinforcement system and identify the "service" loading conditions for repeated loading tests. Fig. 5 illustrates the repeated loading protocols "R1" and "R2" in this table. In particular, the protocol "R1" assumes a constant service load magnitude. On the contrary, the protocol "R2" assumes the increased load magnitude in successive loading repetitions. The latter procedure is typical for the retrofitted specimens NSL-2, ES1–1, and ES1–2 (#14, #21, and #22 in Table 3), where the additional CF reinforcement increased the composite system's load-bearing capacity. The RC beams of elements NSL-2, ES1–1, and ES1–2 were loaded until the theoretical service load before retrofitting. In contrast, the RC beam elements of the test groups ES2 and ES3 (samples #23–#26 in Table 3) were tested near the steel reinforcement yielding moment before strengthening to illustrate the retrofitting effect under different damage conditions in RC structures.

The load cycles created the dataset for regression analysis (**Section 4.3**). After each load cycle set, the specimens were fully unloaded to measure residual deformations. In repeated loading tests, the curvature of the bending zone does not return to zero after

Table 3
Loading parameters of the beam samples [kNm].

Nr.	Beam	Loading protocol*	$\mathbf{M}_{min}$	$\mathbf{M}_{max}$	$\mathbf{M}_{ser}$	$\mathbf{M}_{ult}$
1.	S1L	M	–	–	–	4.245
2.	S2L	M	–	–	–	4.724
3.	S3L-1	M	–	–	–	4.949
4.	S3L-2	M	–	–	–	6.499
5.	EL-1	M	–	–	–	7.035
6.	EL-2	M	–	–	–	8.273
7.	EL-3	R1	3.075	4.125	3.71	7.654‡
8.	EL-4	R1	3.075	4.125	3.71	
9.	NL-1	M	–	–	–	5.100
10.	NL-2	M	–	–	–	6.698
11.	NL-3	R1	3.075	4.125	3.71	5.899‡
12.	NL-4	R1	3.075	4.125	3.71	
13.	NSL-1	R2	0.975	1.350	1.215	1.42†
			1.875	2.475	2.220	–◊
			3.075	4.125	3.710	
14.	NSL-2	R2	0.975	1.350	1.215	1.42†
			0.975	1.350	1.215	–◊
			1.875	2.475	2.212	
			3.075	4.125	3.710	
15.	E-1	R1	3.075	4.125	3.71	7.654‡
16.	E-2	R1	3.075	4.125	3.71	
17.	E-3	R1	3.075	4.125	3.71	
18.	N-1	R1	3.075	4.125	3.71	5.899‡
19.	N-2	R1	3.075	4.125	3.71	
20.	N-3	R1	3.075	4.125	3.71	
21.	ES1-1	R2	1.89	2.60	2.24	4.245‡
			3.415	4.500	3.933	–◊
22.	ES1-2	R2	1.890	2.600	2.240	4.245‡
			3.300	4.575	3.973	–◊
23.	ES2-1	M	–	–	–	4.538
		R1	3.338	4.575	3.973	–◊
24.	ES2-2	M	–	–	–	4.508
		R1	3.338	4.575	3.973	–◊
25.	ES3-1	M	–	–	–	6.983
		R1	5.025	6.750	5.888	–◊
26.	ES3-2	M	–	–	–	7.050
		R1	4.920	6.667	5.888	–◊

*M = monotonic load, R1 = repeated load with a constant loading magnitude in consecutive repetition cycles; R2 = repeated load with the loading magnitude increased in successive cycles; †The element with steel reinforcement tested before the retrofitting (Gribniak et al. [20] identified this load-bearing capacity); ‡Average value of similar elements; ◊Were not tested until failure.

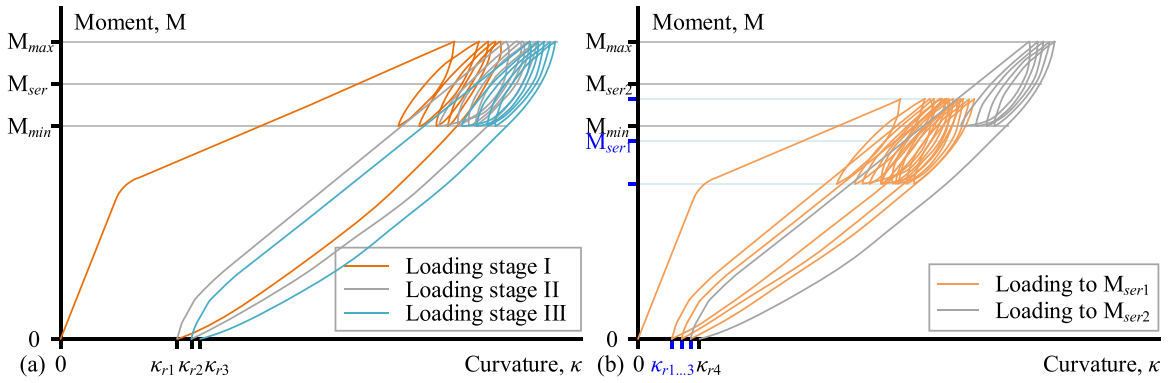


Fig. 5. Repeated loading protocols listed in Table 3: (a) cycling loads over the constant service moment (protocol "R1"); (b) increased intensity load cycles (protocol "R2").

unloading because the concrete-reinforcement system retains residual tensile strain and irreversible microcrack deformation. When continuous monitoring during unloading is not feasible, the residual state is determined from the curvature values recorded 10–20 min after load removal, once the deformation has stabilized. This procedure ensures that the residual curvature is measured consistently across loading stages and provides the reference value required for subsequent stiffness evaluation. In this regard, this approach separates the applied loading from traditional cyclic fatigue tests, which maintain continuous load cycling without complete unloading.

To ensure consistency in the analytical evaluation, the residual curvature measured after each loading stage was used to shift the



Fig. 6. Long-term outdoor exposure of concrete specimens under natural weathering conditions. **Note:** The specimens were stored inverted to maximize exposure to adverse environmental effects.

origin of the moment-curvature diagram, as schematically depicted in Fig. 5. This correction accounted for accumulated deformations and enabled the analytical model described in **Section 3** to adequately assess the composite reinforcement system's residual stiffness, thereby avoiding overestimation due to neglecting accumulated deformations during load repetitions [14,17]. The long-term tests employed similar loading protocols, except that each specimen was subjected to a sequence of repeated loading stages interspersed with environmental exposure intervals. After completing the load cycles, the specimen was exposed to continued open-air conditions outside the laboratory.

2.5. Environmental exposure conditions

To evaluate the long-term durability of composite reinforcement systems under realistic service conditions, a subset of specimens was exposed to natural environmental conditions for up to 3 years. These specimens were placed on the rooftop of the university laboratory building, where they were subjected to the full range of climatic variations characteristic of the Baltic region, including temperature fluctuations, precipitation, freeze-thaw cycles, and UV radiation. Fig. 6 shows the outdoor exposure setup. The EBR, NSM, and EBR-retrofitted specimens (#15–#26 in Table 1) were exposed to the long-term outdoor environment, and pairs of EBR and NSM beams (#7, #8, #11, and #12 in Table 1) were stored under laboratory conditions to provide a reference for comparison.

As shown in Fig. 6, the tension faces of beams with composite reinforcement systems were exposed to sunlight and precipitation, thereby increasing their susceptibility to harmful environmental effects. The specimens were supported on wooden beams to prevent humidity from accumulating beneath them. Throughout the exposure period, the specimens remained undisturbed except during scheduled mechanical testing intervals. At each interval, the specimens were manually removed from the rooftop, subjected to repeated mechanical loading in the laboratory, and then returned to the rooftop.

The environmental exposure conditions were not further accelerated; instead, they relied on natural weathering to reflect realistic service scenarios. Fig. 7**a** shows the characteristic ambient temperature and humidity data (specific measurements and moving-average trendlines) during the exposure period. This approach aligns with the methodology adopted in previous studies [20,38]. At the same time, it provides a representative basis for assessing the long-term performance of composite reinforcement systems using the analytical model described in the next section.

Fig. 7**b** illustrates the number of cross-zero temperature occurrences during the winter of 2022/2023. The data reveal a high average relative humidity (84 %) and 133 freeze-thaw cycles (crossings over 0 °C) within this period. These climatic conditions are consistent with the findings reported by Kliukas et al. [46] , who identified approximately 120 annual freeze-thaw cycles in the Baltic region as typical, with snow cover forming in late October and melting in late March. This quantitative characterization confirms that the environmental exposure conditions in this study are representative of realistic service scenarios.

3. Analytical methodology

This study employs an analytical model and testing procedure previously developed by the research group [14,17,20] that enable the quantification of residual flexural stiffness in reinforced concrete elements subjected to repeated loading. The model interprets the mechanical response in terms of equivalent tensile stresses acting in the concrete, providing a physically meaningful measure of composite efficiency. While the theoretical background and model validation have been presented in earlier publications [14,17,20], this manuscript extends the methodology to analyze long-term stiffness degradation under combined mechanical and environmental exposure, particularly in EBR- and NSM-CFRP systems that are potentially vulnerable to the open environment. The model integrates experimental curvature measurements with a simplified cross-sectional analysis, avoiding iterative procedures and enabling direct evaluation of residual stiffness. To ensure reproducibility and transparency, all relevant equations are included in this section, allowing interested readers to replicate the calculations.

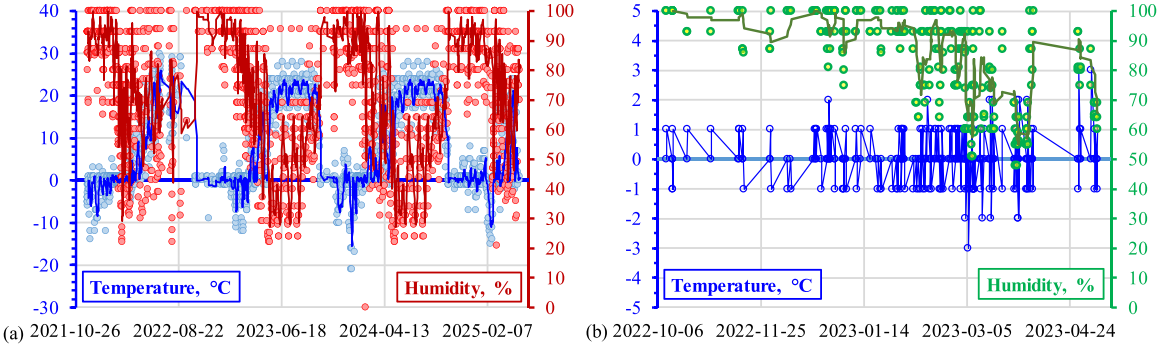


Fig. 7. The characteristic weather conditions: (a) temperature and relative humidity during the environmental exposition period; (b) crossings over 0 °C occurrences and corresponding humidity during the winter of 2022/2023.

3.1. Model description and assumptions

The slab-like geometry of the test specimens (Fig. 2b)—with an extended cross-sectional width and a reduced height—was deliberately selected to promote the formation of multiple cracks in the pure bending zone and to approximate a near-rectangular tensile-stress distribution. This configuration ensures that the entire tension zone of concrete remains effective, as defined in *Eurocode* [40], and enables the use of the smeared-crack concept. The corresponding near-rectangular stress field substantially simplifies the analytical model and allows an explicit solution to the tension-stiffening problem, as established in earlier methodological work [20]. Within this experimentally justified configuration, the analysis follows the classical *Euler-Bernoulli* beam theory, assuming that plane sections remain plane and that shear deformations are negligible, resulting in a linear strain distribution across the height. These simplifying assumptions are applicable for service-load conditions [41], where crack localization, nonlinear concrete behavior, and bond deterioration remain limited. In this context, the analytical formulation provides a coherent basis for expressing residual flexural stiffness in terms of the equivalent tensile stress in concrete (Fig. 1).

The cross-sectional analysis is performed considering the transformed cross-section shown in Fig. 8a. The reinforcement system—whether steel, CFRP, or a hybrid combination—is reduced to an equivalent reinforcement area and modulus of elasticity using Eq. 1, thereby transforming the hybrid configuration into a single component. The effective depth of the reinforcement is calculated as a weighted average based on the stiffness and position of each reinforcement part. Tensile concrete is represented by an equivalent rectangular stress block, as Fig. 8d shows. The equivalent tensile stress, denoted as σ_t*, quantifies the contribution of cracked concrete to overall flexural stiffness. This measure is reinforcement-independent, enabling direct comparison among steel, EBR, NSM, and hybrid systems. The equivalent stress is calculated from the measured curvature and applied bending moment, using the equilibrium conditions for internal forces and moments. The equilibrium conditions of forces and bending moments in the cross-section subjected to the external bending moment M_{ext} (Fig. 8d) determine the model essence:

$$\mathbf{F}_t^* + \mathbf{F}_r - \mathbf{F}_c = 0; \tag{4a}$$

$$\mathbf{F}_r\left(d_r - \frac{h+y_c}{2}\right) + \mathbf{F}_c\left(\frac{h+y_c}{2} - \frac{y_c}{3}\right) - \mathbf{M}_{ext} = 0, \tag{4b}$$

where $\mathbf{F}_t^*$ is the equivalent resultant force in the tensile concrete; $\mathbf{F}_r$ and $\mathbf{F}_c$ are the internal forces acting on the tensile reinforcement and the compressed concrete; d_r is the effective depth of the transformed reinforcement, expressed by Eq. 1. The model also allows the effective depth to exceed the cross-section height (e.g., the $d_r > h$ condition is acceptable for EBR systems).

The system of Eqs. 4a and 4b relates the internal forces and stresses acting on the cross-section, employing the strain compatibility condition (Fig. 8b). Gribniak et al. [20] defined the intermediate solution steps; the final equation describes the third-order polynomial of the neutral axis coordinate y_c for the particular curvature κ and bending moment $\mathbf{M}_{ext}$:

$$\sum_{i=0}^{3} \mathscr{K}_i y_c^i = 0, \tag{5a}$$

with coefficients

$$\mathscr{K}_3 = \frac{E_c b}{6E_r A_r}, \quad \mathscr{K}_2 = 1 + \frac{E_c b h}{2E_r A_r}, \quad \mathscr{K}_1 = h - 3d_r, \quad \mathscr{K}_0 = 2d_r^2 - hd_r - \frac{2\mathbf{M}_{ext}}{\kappa E_r A_r}, \tag{5b}$$

where E_c is the modulus of elasticity of concrete; h and b are the height and width of the cross-section; κ is the average curvature of the pure bending zone; Fig. 8 describes the remaining parameters. This study assumes the modulus E_1 equals E_s (see Table 1), and the following equation determines the modulus of elasticity of concrete [40]:

$$E_c = 22 \bullet \left(f_c'/10\right)^{0.3}, \tag{6}$$

where f'_c is the compressive strength of the concrete cylinders on the first testing day from Table 1.

Eq. 5a has three roots, and the $[0 < y_c \le h]$ condition describes the neutral axis position:

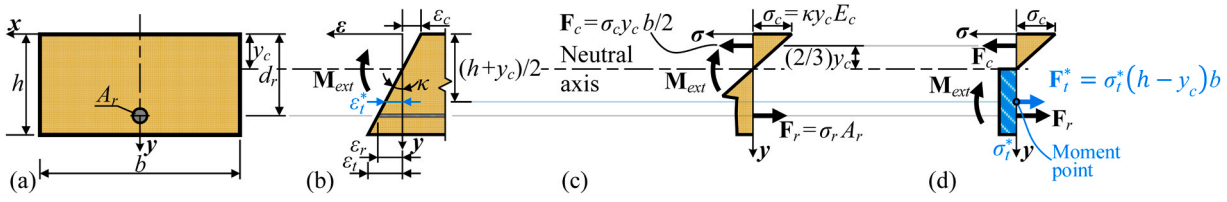


Fig. 8. Analytical model of the stress distribution in the pure bending zone [20]: (a) a transformed cross-section; (b) the bending-induced strain distribution along the cross-section height; (c) the corresponding stress distribution; (d) the equivalent stress approximation in the tension concrete zone.

$$y_c = \frac{2\overline{\mathscr{K}}}{3\mathscr{K}_3}\cos\left(\frac{1}{3}\cos^{-1}\left[-\frac{13.5\mathscr{K}_3^2\mathscr{K}_0 - 4.5\mathscr{K}_3\mathscr{K}_2\mathscr{K}_1 + \mathscr{K}_2^3}{\overline{\mathscr{K}}^3}\right]\right) - \frac{\mathscr{K}_2}{3\mathscr{K}_3}, \tag{7a}$$

$$\overline{\mathscr{K}} = \sqrt{\mathscr{K}_2^2 - 3\mathscr{K}_3\mathscr{K}_1}. \tag{7b}$$

Eq. 5b defines the corresponding coefficients.

The following explicit formulas determine the equivalent stress (Fig. 8d) and average strain of the concrete in tension (Fig. 8b):

$$\sigma_t^* = \kappa\frac{y_c^2 bE_c - 2(d_r - y_c)E_rA_r}{2(h - y_c)b}, \tag{8a}$$

$$\varepsilon_t^* = 0.5\kappa(h - y_c). \tag{8b}$$

The above expressions solve the deformation problem independently of the loading history, explicitly expressing the equivalent stress σ_t* as a function of the bending moment $\mathbf{M}_{ext}$, the average curvature in the pure bending zone κ, the cross-section geometry (Fig. 8a), and the material parameters (Table 1). In this study, the equivalent stress serves as a scaled measure of the composite reinforcement's bending stiffness. As it approaches zero, this measure indicates the absence of the composite effect of reinforcement. This assumption aligns with the principles of composite mechanics, e.g., [47,48]. Negative stress values indicate that the simplifying modeling assumptions (e.g., elastic material behavior) are invalid.

Further extensions involving non-linear effects are possible (e.g., [17,39]). However, these elaborations complicate the modeling procedure and typically require iterative calculations and a loading history, making them not feasible for engineering applications. At the same time, because the geometry of the bending specimens (Figs. 2b and 3a) was intentionally adapted to promote smeared cracking and a near-rectangular tensile-stress field, these relatively small elements cannot serve as substitutes for full-scale beam tests and are primarily suitable for material-oriented characterization, with emphasis on the interaction between reinforcement and concrete.

3.2. Evaluation of residual bending stiffness

This section illustrates how experimental measurements are transformed into equivalent stresses using the analytical model. The examples provided are explanatory and do not represent the complete dataset analyzed in **Section 4**.

The evaluation of residual bending stiffness in this study is based on transforming experimentally measured load-displacement data into moment-curvature diagrams, which serve as input to the analytical model described in **Section 3.1**. The vertical displacements were measured at multiple points along the beam span (Fig. 4a), including the pure bending zone defined by the loading and support locations. The external bending moment was computed from the applied load and the known geometry of the four-point bending setup. The curvature in the pure bending zone was calculated using a finite-difference approximation based on the vertical displacements recorded by LVDTs, as described by Eq. 2. The surface deformations captured by the DIC system (Fig. 5a) were used to verify the curvature assessments, using Eq. 3.

Fig. 9 illustrates how experimental measurements are transformed into moment-curvature diagrams. Fig. 9a shows the vertical

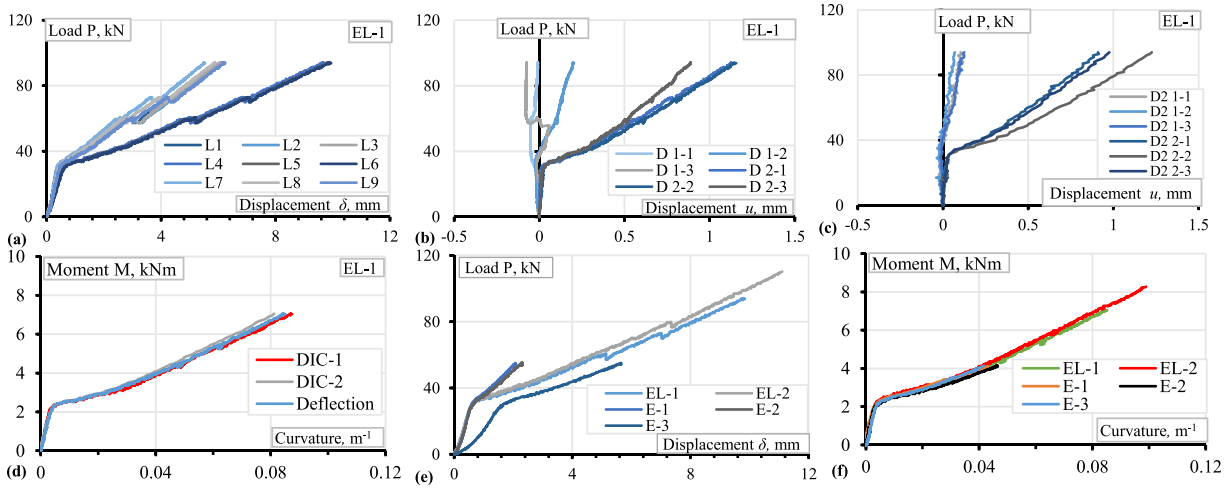


Fig. 9. Experimental measurement results: (a) vertical displacement diagrams of the EL-1 beam sample; (b) and (c) the deformation distribution captured by DIC at the side surfaces of the EL-1 beam; (d) the corresponding curvatures determined using vertical and side deformations; (e) and (f) the vertical displacements at the mid-span and the corresponding moment-curvature diagrams of selected EBR specimens subjected to the short-term mechanical load.

displacements of specimen EL-1 captured by eight LVDTs positioned beneath the beam (Fig. 4a). Figs. 9b and 9c present strain distributions recorded on the side surfaces; because the measurement lines span both tension and compression zones (Fig. 4a), the diagrams include negative values corresponding to compressive strains. Fig. 9d combines these measurements (Figs. 9a–9c) into moment-curvature relationships using Eqs. 2 and 3. Figs. 9e and 9f illustrate how this transformation reduces scatter in short-term test results for nominally identical beams.

Considering the repeated-load procedure (Fig. 5), the residual curvature is the essential parameter to be included in the residual stiffness analysis. In this context, the residual curvature acts as a reference shift in the curvature, ensuring that each loading stage is interpreted relative to the deformation state accumulated during previous repetitions and not to an unrealistically zero-curvature configuration. Therefore, the moment-curvature relationships were constructed for each loading stage, with the diagram origin shifted to account for residual curvature accumulated during previous cycles. Fig. 10a shows this modification procedure for the moment-curvature diagrams of the selected specimens. The equivalent tensile stress in the concrete, σ_t*, was calculated using Eq. 8a, which relates the bending moment and curvature to the internal force equilibrium in the cross-section. The corresponding average tensile strain, ε_t*, was determined using Eq. 8b. These values provide a consistent, physically meaningful measure of the composite system's residual stiffness. Fig. 10b shows the equivalent stress-strain diagrams corresponding to the moment-curvature relationships in Fig. 10a. These diagrams illustrate the stiffness regime relevant to this study, where the evaluation is restricted to service-load conditions and does not extend into the post-yield range. In this context, the equivalent tensile stress σ_t* serves as the indicator of the composite action between concrete and reinforcement. Values of σ_t* within the elastic range reflect the mobilized interaction, whereas decreasing values indicate a progressive loss of composite efficiency with repeated loading. For specimen ES1–1, the additional stage "Loading-0" corresponds to the initial test of the beam with only steel reinforcement, before retrofitting. Subsequent stages ("Loading-I" onward) reflect the behavior of the retrofitted element.

While the diagrams shown in Fig. 10b offer insight into the mechanical behavior of the composite systems, direct comparisons across different reinforcement configurations are complicated by variations in reinforcement stiffness, geometry, and bond characteristics. However, equivalent stress-strain diagrams should be constructed for each loading stage, using load cycles to visualize the evolution of this parameter and to generate a database for regression analysis [14]. Following the approach adopted in previous studies [17,20,38], this investigation focuses on a specific loading level—referred to as the service load—to enable consistent comparison of residual stiffness across specimens. To ensure statistical robustness and minimize the influence of measurement noise, the specimens #7, #8, and #11–#26 (Table 3) were subjected to multiple (five) load cycles over the service moment. These cycles were designed to fluctuate around the target (service) load level. The repeated measurements allowed the identification of trends in stiffness degradation and the estimation of average equivalent stress values at the service load level [14].

Fig. 11 illustrates the transformation of the moment-curvature diagrams under repeated load cycles (Fig. 11a) into the equivalent stresses trendlines (Fig. 11b) of the selected specimens. Notably, the first data point of the first loading cycle was excluded from the regression analysis. This decision was made to eliminate the influence of initial cracking, which typically results in a disproportionately low curvature and may distort the regression trends. The remaining data points—particularly those corresponding to the ascending branches of the load cycles—were used to construct the residual stress diagrams and to evaluate the decay of flexural stiffness with load repetitions (Fig. 11b). To ensure consistency in trendline generation, identical rules were applied to all specimens and loading stages. Only the ascending branches of the load cycles (Figs. 5 and 11a) were considered in the regression analysis, because they provide a stable curvature-moment relationship unaffected by unloading-related scatter. The five consecutive load cycles performed at each stage produced multiple curvature measurements at the predefined service-load level, enabling a statistically representative estimate of σ_t* without excessive data inflation. As a result, each trendline in Fig. 11b reflects the averaged mechanical

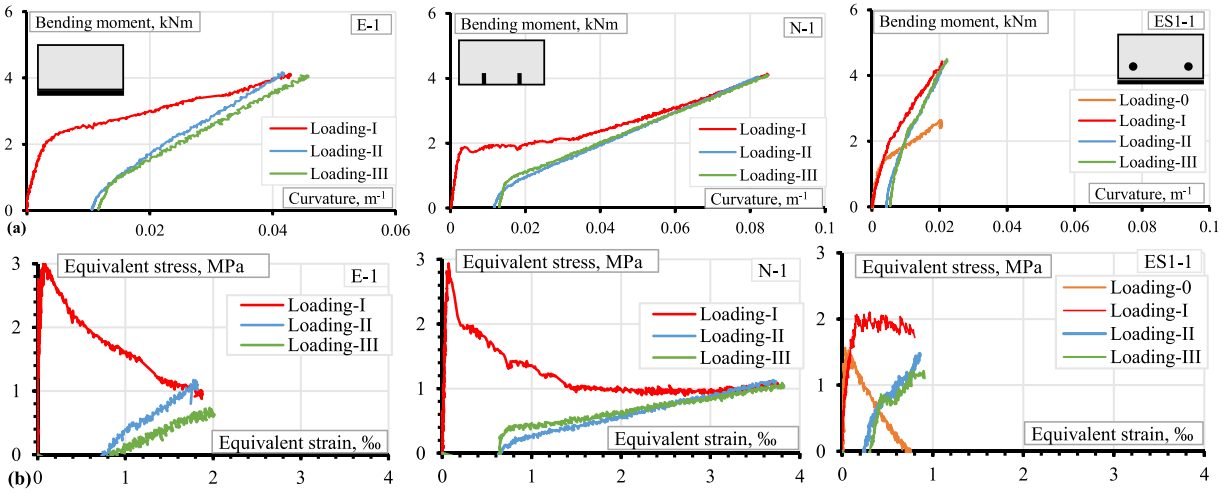


Fig. 10. Results of selected EBR, NSM, and retrofitted beams corresponding to different load repetitions: (a) moment-curvature diagrams; (b) the corresponding equivalent stress-strain diagrams (**Eq. 8**).

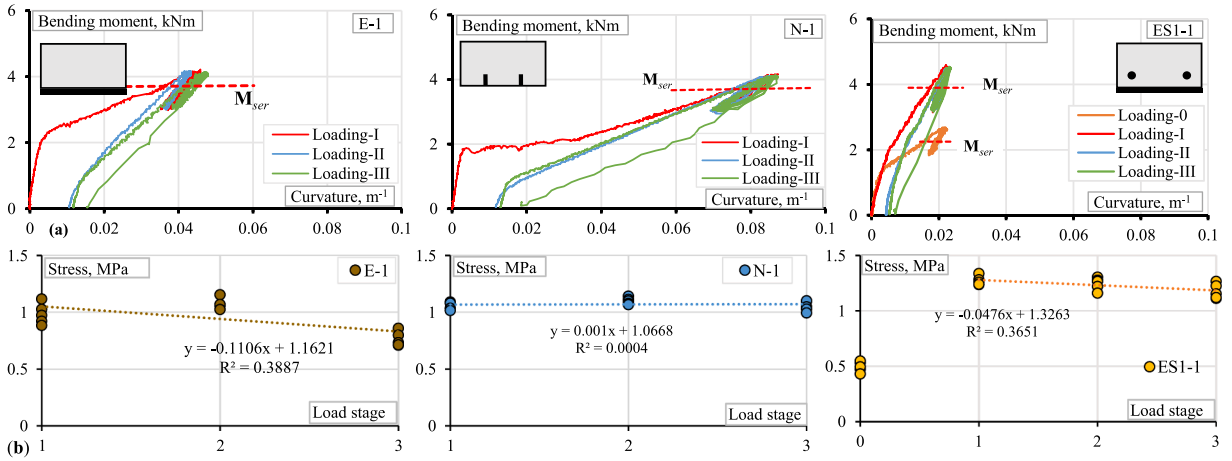


Fig. 11. Results of selected EBR, NSM, and retrofitted beams corresponding to different load repetitions and loading cycles: (a) moment-curvature diagrams; (b) the corresponding trendlines of the equivalent stress-strain diagrams at the service load level.

response corresponding to the same reference load and is independent of local variations in cracking or temporary stiffness fluctuations.

By tracking the evolution of σ_t* over successive loading stages, it is possible to identify long-term trends in stiffness. It is important to emphasize that the comparison of stiffness trends is performed exclusively at the predefined service-load level (e.g., Fig. 11a). This fixed mechanical demand ensures that the evolution of σ_t* reflects changes in composite action rather than differences in loading magnitude. All trendlines (e.g., Fig. 11b) include the corresponding regression equations and determination coefficients, where slopes approaching zero indicate the absence of a measurable parametric effect, and the determination coefficients quantify the proportion of variation attributable to changes in loading stage or exposure duration. Section 4.3 discusses the long-term stress degradation trends in more detail. The loading stage designated as "Loading-0" in Fig. 11 corresponds to the testing of the RC beam that was retrofitted with the EBR system afterwards. This load was not included in the regression analysis. The increase in the stiffness in this case results from the neglect of the residual curvature of the RC beam, as discussed in Section 2.4.

4. Results and discussion

This section presents and interprets the experimental results obtained from the short-term and long-term testing phases. The analysis is grounded in the equivalent tensile stress values derived from the analytical model described in **Section 3.1**. The discussion begins with the short-term performance of the specimens, focusing on the applicability and limitations of the proposed methodology. Subsequent subsections address the long-term degradation trends, the influence of reinforcement configuration, and the effects of environmental exposure on the residual stiffness of the composite reinforcement systems. The results are supported by moment-curvature and equivalent stress-strain diagrams, as well as regression analyses of residual stiffness decay. The following discussion interprets the evolution of stiffness strictly at the service-load level, consistent with the analytical framework established in **Section 3**.

4.1. Short-term performance comparison

Fig. 12 shows the load-vertical displacement diagrams at the midspan of the monotonically loaded beam specimens—the elements

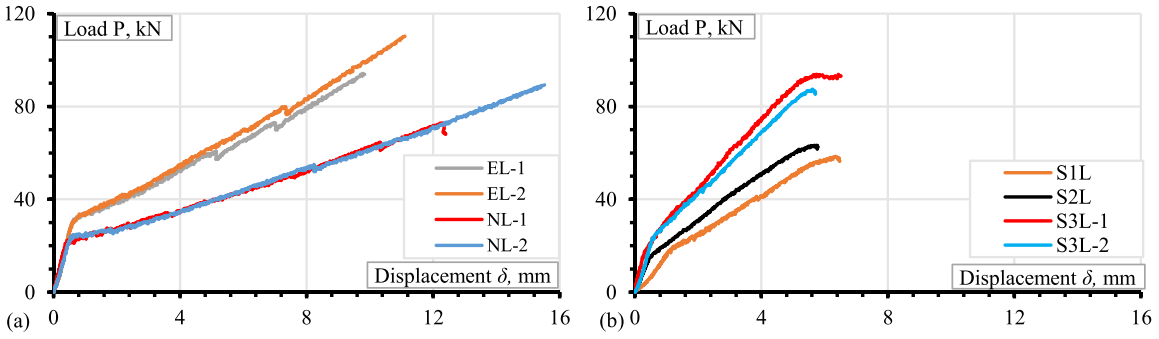


Fig. 12. Load-vertical displacement diagrams of the beam samples subjected to monotonic load.

with steel and CFRP reinforcement exhibit distinct load-displacement curves and failure mechanisms. The specimens with steel reinforcement failed in flexure due to the steel bar yielding. On the contrary, shear failure terminated the bending tests of the element reinforced with CFRP strips and CF sheets. On the one hand, this test outcome results from the high tensile strength of CF materials (Table 2). On the other hand, these materials are prone to carrying tension into the fibers and are weak at resisting loads orthogonal to

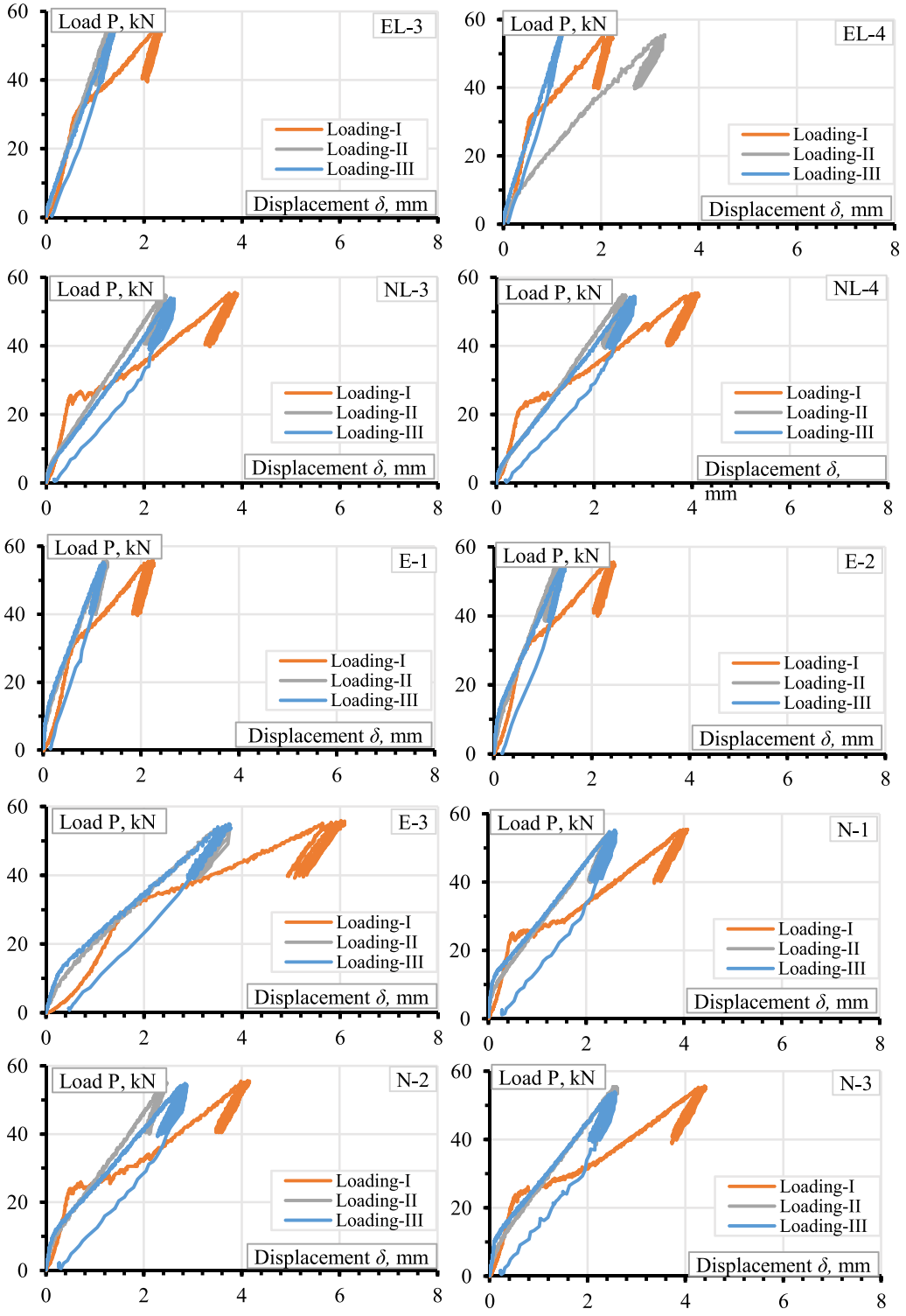


Fig. 13. Load-vertical displacement at the mid-span diagrams of NSM and EBR beams subjected to repeated load protocols (Table 3).

the fibers. However, these failure mechanisms are beyond the scope of this investigation, which focuses on the service loading conditions. Gribniak et al. [8,20] investigated these mechanisms in detail, which are not repeated here to avoid obscuring the innovative aspect of this study, which focuses on the analysis of the residual flexural stiffness of composite systems.

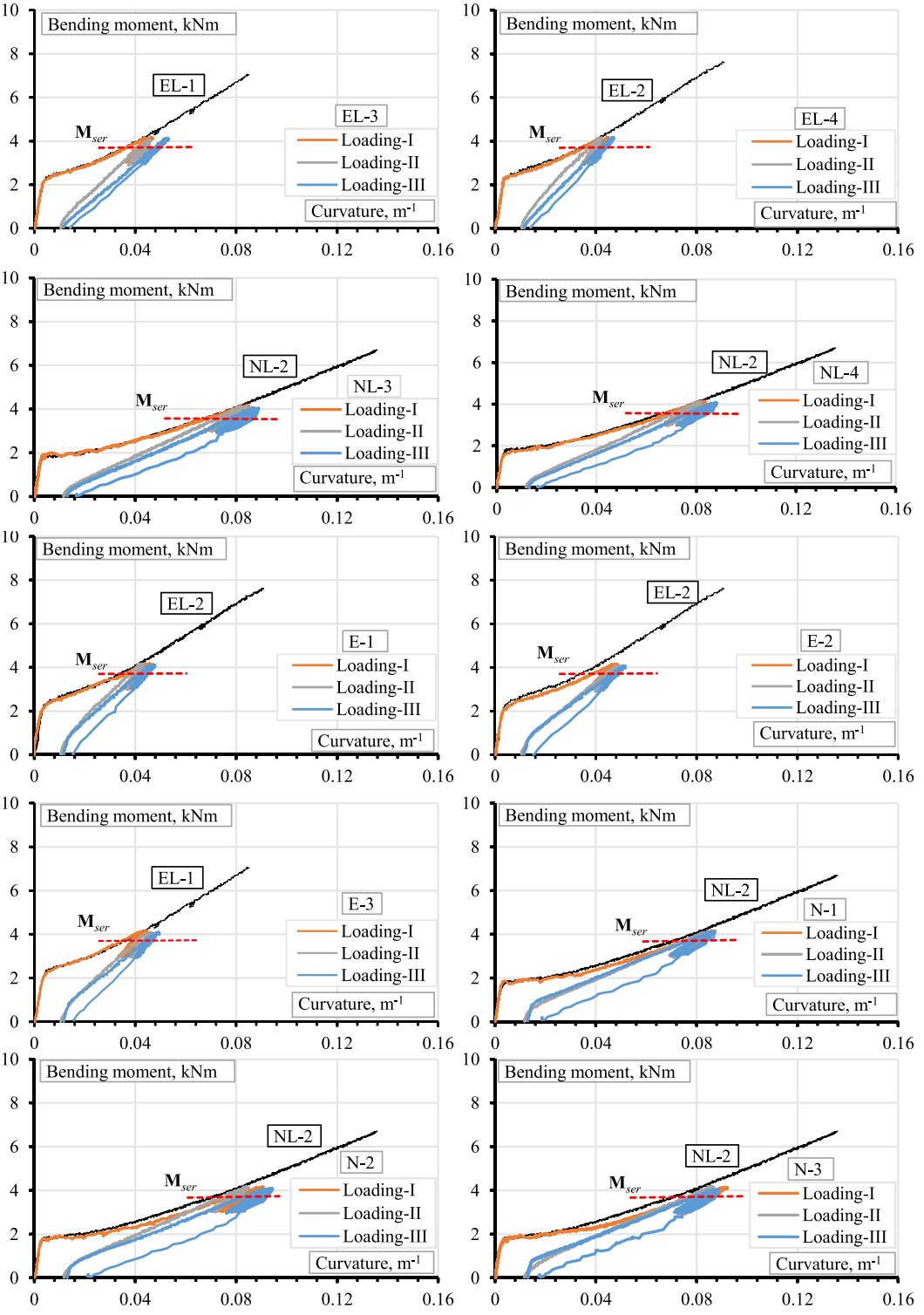


Fig. 14. Moment-curvature diagrams of the NSM and EBR specimens subjected to repeated load cycles. **Note:** Dashed red lines indicate the reference service load level used for stiffness comparison.

Another aspect that Fig. 12 reveals is the load-bearing capacity of composite-reinforced beams, which substantially exceeds that of steel-reinforced counterparts, despite the opposite trend in the reinforcement ratio $n\rho$ (Table 1). At the same time, the Model Code 2020 [49] introduces a simple deflection limit of $L/250$ (L = span of 900 mm, Fig. 4a), resulting in a 3.6 mm deflection limit for the test samples in Fig. 12. Considering this deformation limit, the NSM (Type NL) specimens with $n\rho = 0.7$ % are equivalent to the beam S1L ($n\rho = 3.3$ %), and EBR (Type EL) elements are comparable to the beam S2L with $n\rho = 3.8$ %. This analysis compares the mechanical efficiency of composite reinforcement systems with that of ordinary steel bars. Combining steel and CFRP materials reduces the deformability. Further, it enhances the mechanical performance of the reinforcement, enabling it to exceed the steel's yielding deformation limit without compromising structural safety and efficiently utilizing structural material [3,9,20], which is the focus of further research.

4.2. *Load repetitions and moment-curvature behavior*

The proposed methodology enables engineers to evaluate the residual stiffness of reinforced concrete elements subjected to repeated loading, including not only mechanical but also environmental and temperature effects. Sultani et al. [14] and Gribniak et al.

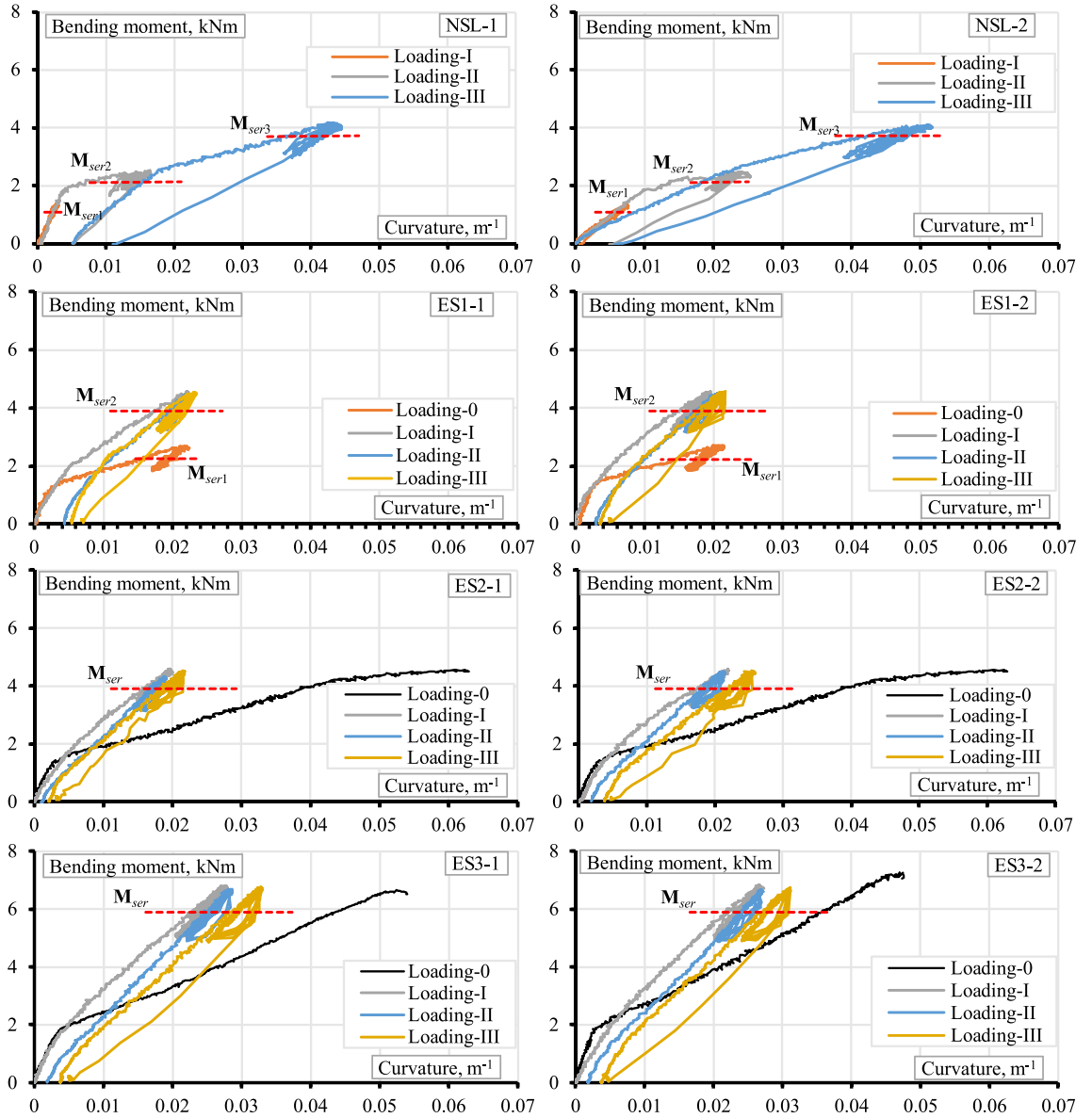


Fig. 15. Moment-curvature diagrams of the RC specimens strengthened with CF materials and subjected to repeated loading cycles. **Note:** Dashed red lines indicate the reference service load level used for stiffness comparison.

[17,20,39] demonstrated that the analytical model can capture the combined influence of elevated temperature and mechanical cycling, provided that the residual deformation—expressed as curvature—is accurately recorded.

A critical aspect of this methodology is the treatment of residual deformation. Each subsequent loading stage must begin from the residual deformation state accumulated during the previous stage. This shift in the origin of the moment-curvature diagram (Figs. 5 and 10a) is essential for correctly estimating the equivalent tensile stress and, by extension, the residual stiffness. For example, Fig. 13 shows the load-displacement diagrams of NSM and EBR specimens subjected to repeated loading protocols (Table 3). These diagrams can be treated as typical outcomes of experimental studies when only mid-span deformation is recorded, and residual deformations are neglected. Failing to shift successive diagrams (Fig. 13) creates an unrealistic impression of increased stiffness. In particular, the consecutive diagrams localized at the coordinate origin showed a reduction in deformations relative to the first loading step, artificially increasing the expected reinforcement effect under repeated loads.

In addition, mid-span deformations may result in different responses among nominally identical beams (e.g., E-2 and E-3, Fig. 13). Gribniak et al. [20] attributed this discrepancy to an uneven distribution of deformation within the composite reinforcement system. Averaging curvature within the pure bending zone equalizes the deformation response of the beam samples (e.g., Fig. 9f), making these diagrams suitable for stiffness analysis. Therefore, this study employs a twofold transformation of load-displacement diagrams of composite elements subjected to repeated mechanical loads, illustrated in Figs. 10 and 11. The load-displacement diagrams (e.g., Fig. 13) are transformed into moment-curvature diagrams and distributed (shifted from the coordinate origin) according to the residual curvature values. Figs. 14 and 15 show the transformed moment-curvature diagrams prepared for the stiffness analysis. The "Loading-0" in Fig. 15 denotes the mechanical test performed on the original steel-reinforced beam before applying the CFRP strengthening system.

Fig. 14 also includes the reference specimens (of the same reinforcement type) tested under monotonic load to prove the

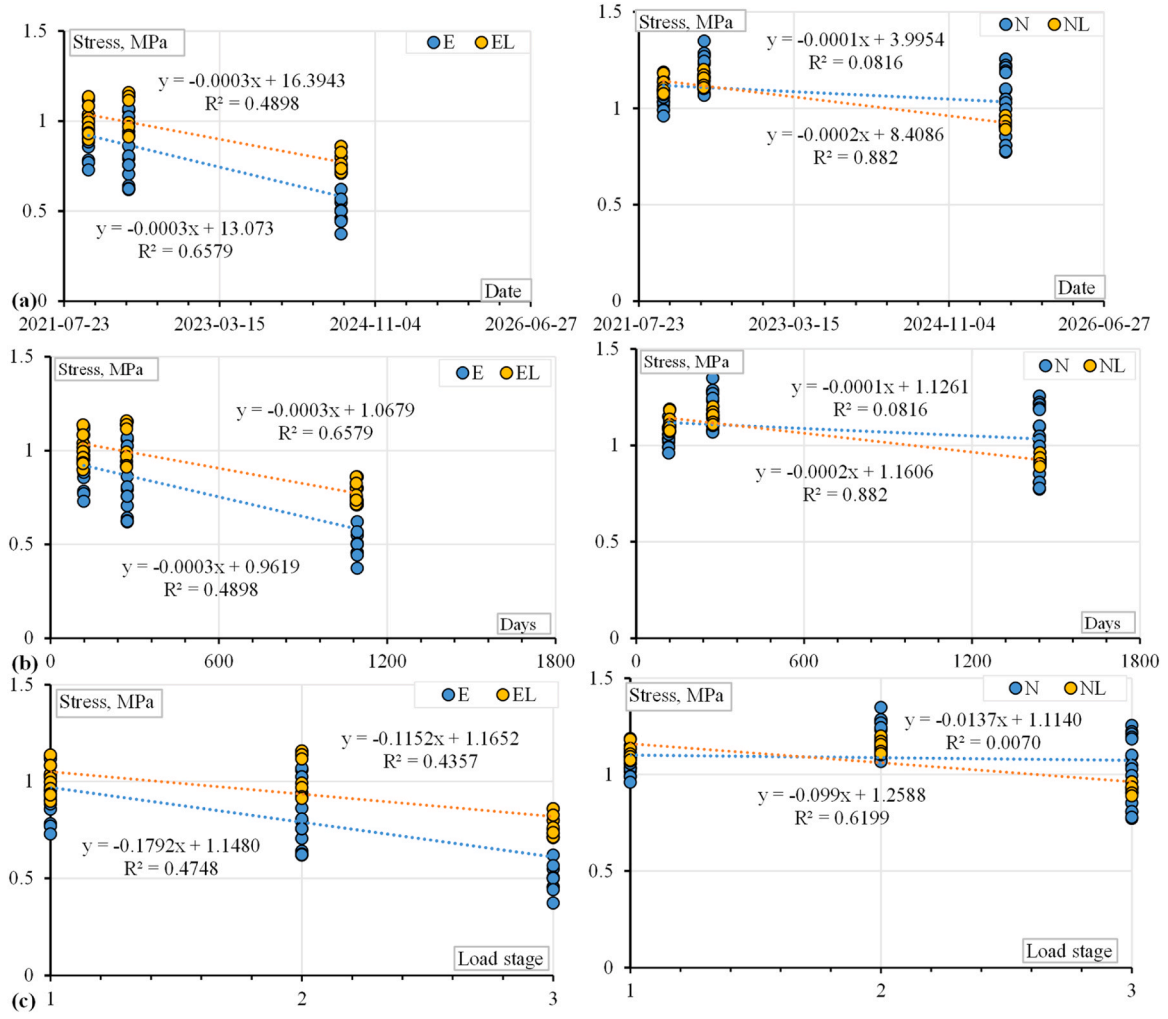


Fig. 16. The regression trends of the equivalent stresses of the EBR and NSM specimens stored in the laboratory and exposed to the open environment: (a), (b), and (c) the trendlines related to the testing date, storing duration, and load repetitions, respectively.

consistency of the applied moment-curvature transformation. As discussed in **Section 4.1**, the stiffness of the EBR specimens outperforms the NSM elements. This difference in the reinforcement ratio $n\rho$ (1.0 % *vs.* 0.7 %) can explain this observation. At the same time, quantifying stiffness decay due to repeated loading and long-term effects is difficult to assess using these diagrams.

The developed analysis approach also presents a challenge when analyzing specimens that were strengthened after initial mechanical testing. In the case of retrofitted specimens (Fig. 15), the diagram's origin cannot be unambiguously defined. Associating the origin with the residual deformation of the tested RC element (referred to as "Loading-0") neglects the fact that the newly applied CFRP reinforcement (sheets or strips) has no prior deformation history. Conversely, setting the origin at zero curvature ignores the residual deformation of the RC member before strengthening. Both approaches introduce a degree of simplification and potential inaccuracy. In this study, the second approach was adopted, which may slightly overestimate the residual stiffness of the retrofitted specimens.

The service load level is introduced for comparison purposes, as described in **Section 3.2**. Figs. 14 and 15 indicate this level using dashed red lines. This reference point allows the evaluation of residual stiffness at a fixed mechanical demand, independent of the environmental condition or prior loading history. Previous studies [20,38] and the present investigation have shown that both EBR and NSM systems are susceptible to environmental conditions. These findings motivated the selection of EBR, NSM, and those hybrid (retrofitted) systems for long-term testing in this study.

4.3. *Stiffness degradation trends*

The long-term performance analysis focused on the evolution of residual flexural stiffness, expressed as the equivalent tensile stress σ_t*, at the service load level (Fig. 11). This approach enabled a consistent comparison of stiffness degradation across different reinforcement systems and loading and storage conditions. The following analysis aggregates the equivalent stresses determined from Figs. 14 and 15. In other words, it combines the results from nominally identical specimens stored under the same conditions (inside or outside the laboratory) and treats them as a single dataset. Fig. 16 shows the regression trends for the EBR and NSM systems stored in laboratory conditions and exposed to the open environment. As defined in **Section 3.1**, the equivalent tensile stress σ_t* represents the mobilized composite action of the concrete-reinforcement system; therefore, decreasing values of σ_t* signify a progressive loss of composite efficiency, while values approaching zero indicate that the interaction within the composite system has vanished. In Figs. 16**a** and 16**b**, the coordinate origin corresponds to the day of concrete pouring. Thus, the trendlines quantify the degree to which composite action is preserved or lost under repeated loading and environmental exposure.

Fig. 16 reveals an apparent distinction between the long-term behavior of NSM and EBR systems. Specimens reinforced with NSM strips exhibited nearly identical residual stiffness trends, whether stored under laboratory conditions (the "NL" group) or exposed to the open environment (the "N" group). When only mechanical load repetitions are considered (Fig. 16**c**), the N-type specimens exhibit an almost horizontal regression line, which indicates that repeated loading had no measurable influence on residual stiffness (expressed as equivalent tensile stress σ_t*) in NSM reinforcement systems. The determination coefficient (R^2) of this regression model also approaches zero. Considering load duration (Figs. 16**a** and 16**b**), some negative inclination of the trendline appears, but it is insignificant in a statistical sense (considering the scatter of the stiffness measurement points). This consistency confirms that the NSM systems are largely unaffected by environmental conditions. This mechanical stability can be attributed to the embedded configuration of the NSM strips, which protects the adhesive interface from harmful environmental effects, thereby mitigating the deterioration mechanisms that typically affect surface-bonded CFRP systems [35].

In contrast, EBR systems demonstrate a noticeable decrease in the residual stiffness. Remarkably, both considered factors, i.e., storage duration (Figs. 16**a** and 16**b**) and load repetitions (Fig. 16**c**), affect the stiffness losses. Moreover, environmental storage conditions also accelerate the decrease in stiffness. After approximately 1000 exposure days, the differences in residual stiffness became significant (the measurement points of the "E" and "EL" groups do not overlap). On average, this difference is equal to 20 %. This behavior underscores the known vulnerability of EBR systems to environmental degradation, particularly because the adhesive layer is directly exposed to moisture, temperature fluctuations, and UV radiation [17,20]. These observations agree with recent durability studies [34,35,50–52], which reported that surface-bonded CFRP systems experience progressive interfacial weakening due to epoxy aging, moisture ingress, and hygrothermal cycling, impairing stress transfer and leading to measurable long-term reductions

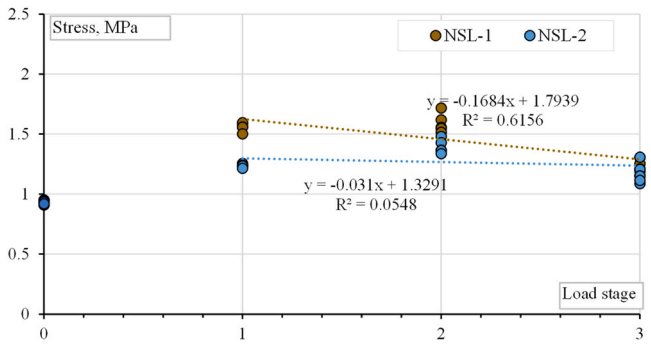


Fig. 17. Equivalent stresses of the hybrid and retrofitted specimens stored in laboratory conditions.

in composite action. Although the susceptibility of EBR systems to environmental effects is well documented [18,19,27,29,50,53,54], the methodology presented in this study offers a novel advantage: it enables quantification of stiffness degradation in a physically interpretable and reproducible manner. By focusing on equivalent tensile stress at a defined service load level, the approach provides engineers with a practical tool for assessing the long-term performance of composite reinforcement systems and for making informed decisions in the design and rehabilitation of concrete structures.

Despite computational efficiency, the developed approach introduces some simplifications. Simplified material models enable the model to estimate residual stiffness under service loads [14,17,20]. However, the repeated loading condition requires adequate capture of residual curvatures to ensure adequate evaluation of residual stiffness (Fig. 5). This analysis is not trivial for estimating the residual stiffness of the retrofitted specimens. The hybrid reinforcement specimens NSL-1 and NSL-2 illustrate this complexity. Fig. 17 shows the corresponding residual stiffness analysis results, which reveal the effect of neglecting the residual deformations of the NSL-2 beam sample. This element was tested as an RC sample before retrofitting, while the NSL-1 beam was strengthened before the mechanical tests. All remaining characteristics of these beams have remained unchanged.

Fig. 17 shows the distinct trends of potentially identical specimens. The reference hybrid reinforcement sample (NSL-1) shows stiffness degradation comparable to the NSM results shown in Fig. 16**c**; compare the inclination coefficients of the trendlines: –0.168 (NSL-1) and –0.099 (NL-type samples in Fig. 16**c**). The results of the NSL-2, retrofitted after the first mechanical load ("Loading-0" in Fig. 15 and the load stage "0" in Fig. 17), demonstrate no stiffness degradation signs: the inclination coefficient –0.031 approaches zero. Moreover, the second loading repetition results in an increase in stiffness (regarding the first loading stage). The diverse estimated trends in σ_t* for the NSL-1 and NSL-2 samples (Fig. 17) result from neglecting the NSL-2 samples' initial curvature before the CF EBR sheets were applied. This inaccuracy is already detectable at a relatively low reinforcement ratio ($n\rho$ = 1.83, Table 1) and may increase with higher reinforcement ratios and loading intensities. The resulting error cannot be explicitly reduced and must be accounted for when analyzing the residual stiffness of retrofitted specimens. This aspect must be taken into account when analyzing the residual stiffness results for the retrofitted specimens subjected to long-term environmental exposure outside the laboratory, i.e., the beam samples #21–#26 in Tables 1 and 3. Fig. 18 shows these results along with the E-type EBR elements. These results demonstrate the prominence of the hybrid reinforcement systems and the retrofitting effect of the EBR systems.

The following noticeable aspects emerge from the results of Fig. 18:

- *The ES2 and ES3 type beams*. Increasing the reinforcement ratio (the $n\rho$ of the hybrid system increased from 4.0 % to 6.6 %; Table 1) improves residual stiffness, with equivalent stresses exceeding 1 MPa in the long term, or over 40 % (using the ES2 samples as a reference). The ES3-type elements also demonstrate immunity to long-term environmental exposure, with the inclination coefficient of the duration trendline approaching zero. This conclusion underscores that, despite the earlier criticism of EBR systems when used alone, their combination with steel reinforcement significantly enhances mechanical efficiency, making externally bonded CF sheets a viable solution even under challenging environmental conditions.
- *The ES1 and ES2 type beams*. Even with a higher reinforcement ratio (4.3 % vs. 4.0 %, Table 1), the ES1-type beams exhibit substantially lower residual stiffness, as evidenced by a 1 MPa difference in the equivalent stresses, reflected in a vertical shift of the trendlines. This result is not surprising, given that the ES2-type beams were retrofitted after the steel reinforcement reached its yield limit; in contrast, the ES1-type specimens were retrofitted after reaching the service moment, as shown in Fig. 15. In other words, neglecting the residual curvature resulting from loading level "0" causes the stiffness estimation difference. This case exemplifies the limitations of the analytical model in estimating "true" stress values after retrofitting the damaged specimens. However, despite this limitation, the model explicitly captures the long-term tendencies in the equivalent stiffness decay.
- *The EBR (E-type) and hybrid systems.* This comparison represents a controlled scenario that illustrates the analytical approach's sensitivity. Notwithstanding its artificial nature, this situation exemplifies the sensitivity of the proposed analytical approach to quantifying the residual stiffness of the composite reinforcement system. In particular, the scatter in the equivalent stresses over the

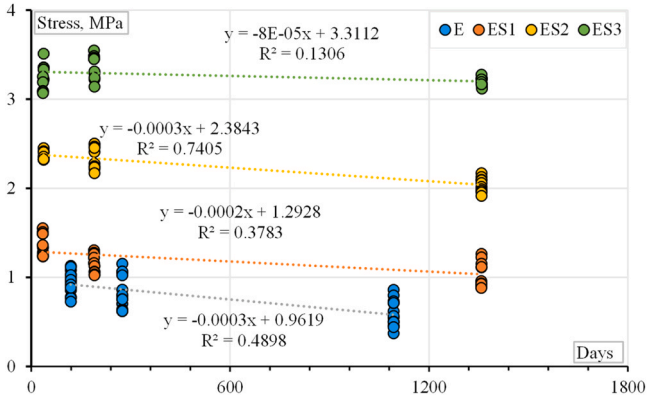


Fig. 18. Equivalent tensile stress versus exposure duration for retrofitted hybrid systems and EBR specimens under open-air environmental conditions.

long term decreases with the introduction of steel reinforcement, and the proposed model can quantify this effect. This quantification is essential and paramount for assessing the structural resistance's reliability and provides a reliable tool for analyzing it under environmental conditions.

An increasing number of cracks in the bending zone indicates the ability of the composite reinforcement system to mobilize the concrete's tensile capacity. It thus demonstrates effective composite interaction [41]. Fig. 19 illustrates the cracking process in the pure bending zone of specimen ES2-1 before and after retrofitting. The cracks were localized using the DIC technique (Fig. 4**b**). Before strengthening, 11 cracks formed within the 600 mm bending zone (Fig. 4**a**) at the ultimate load (Table 3). After retrofitting, the crack count increased to 17, producing a denser pattern with an average spacing reduction from 50 mm to 33 mm. On the one hand, the appearance of new cracks after strengthening confirms that the concrete continues to resist tensile stresses under mechanical loading, which reflects the mechanisms contributing to the increased mechanical resistance of the retrofitted beam (Fig. 15). On the other hand, the resulting dense, smeared crack distribution—characteristic of the slab-like beam samples intentionally designed to densify crack spacing [20]—limits the applicability of these observations for modeling real-scale beams, where crack patterns are typically sparse and dominated by localization phenomena [41].

The limited number and configuration of the experimental samples also ensure that only general tendencies are captured. Building on these experimental observations, the following section situates the findings within the broader context of existing literature.

4.4. Comparative discussion with literature

The proposed residual stiffness analysis offers a practical and scalable approach for comparing the long-term performance of composite reinforcement systems under realistic conditions. While the present results (e.g., Fig. 16) confirm several observations previously noted in experimental and analytical investigations [14,17,20], they also highlight critical gaps in the current literature regarding stiffness degradation under combined mechanical and environmental actions.

The superior performance of NSM systems under environmental exposure conditions is consistent with previous studies [4,19,55]. This resilience is primarily attributed to the partial embedment of CFRP strips, which improves protection against moisture ingress and UV radiation. However, most available investigations focus on ultimate strength or bond durability rather than on the evolution of stiffness under service load conditions. Few studies [14,56] quantify residual stiffness using physically interpretable measures such as equivalent tensile stress, leaving a gap in understanding the progressive stiffness decay in NSM systems subjected to repeated loading and natural weathering. Future research should address this gap by integrating curvature-based evaluation methods into long-term durability studies.

The accelerated stiffness decay observed in EBR systems corroborates prior reports on the susceptibility of externally bonded CFRP sheets to environmental stressors such as UV radiation, thermal cycling, and moisture ingress. Although numerous studies [16–19,25,27,29,50,53,54] have examined bond strength deterioration, few have established a clear link between these findings and stiffness-based performance indicators. For example, investigations by Cruz et al. [50] and Dushimimana et al. [18,54] emphasize adhesive degradation but do not establish a systematic link between adhesive degradation and loss of flexural stiffness under repeated mechanical loading. This disconnect underscores the need for integrated methodologies that couple bond durability with stiffness quantification at service load levels.

Hybrid reinforcement systems showed promising results in this study (Figs. 17 and 18), confirming previous observations [5,9,21–24,57]. Yet, their long-term performance under combined environmental exposure and repeated loading remains insufficiently documented in the literature. This gap highlights the need for standardized approaches to quantify stiffness retention in hybrid configurations [9,21,58,59]. Moreover, the effect of prior damage and residual curvature on stiffness evaluation—illustrated by the NSL and ES series in this study—has received limited attention in previous work [14,17,20], despite its practical relevance for retrofitting strategies.

Most published research relies on ultimate capacity or load-deformation response, which fails to capture progressive stiffness degradation [31,32,34,35]—a gap addressed by the equivalent tensile stress approach proposed in this study. These metrics, while

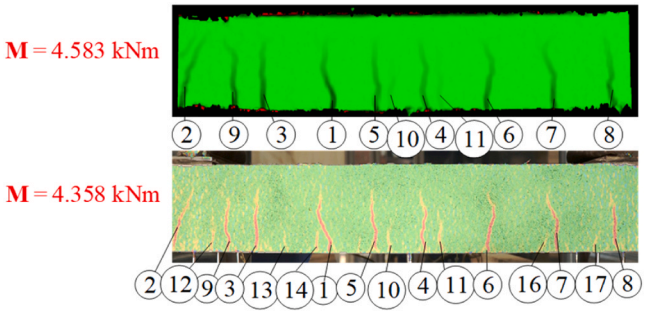


Fig. 19. Crack patterns in the pure bending zone of the selected ES2–1 specimen before (top image) and after retrofitting (bottom image). **Note:** The numbers indicate the cracking sequence.

useful for strength assessment, fail to capture subtle yet critical changes in stiffness that influence serviceability and long-term reliability. Recent reviews [31,51,52,60–62] have called for performance-based indicators that reflect structural efficiency under realistic service conditions. The equivalent tensile stress approach adopted in this study addresses this need by providing a scalable, physically interpretable measure of stiffness degradation, which can be integrated into durability-based design frameworks.

A key innovation of this study is the highlighting of the significant influence of residual curvature in pre-damaged elements on post-retrofitting stiffness (Fig. 18). Only the previous publication by this research team [14] raised this problem. However, this publication only mentioned this effect without systematically illustrating the artificial increase in estimated stiffness, as demonstrated by the NSL, ES1, ES2, and ES3 groups of specimens in Figs. 15, 17, and 18. This specific aspect of the structural behavior of retrofitted elements is necessary for accounting in the practical application of the proposed analytical approach to the residual stiffness analysis.

Despite advances in FRP technology, the long-term mechanical reliability of composite reinforcement systems remains insufficiently documented, particularly under combined mechanical and environmental actions. Key research needs include [19,31,50,60,61]:

- Development of standardized test protocols for stiffness evaluation under repeated loading and natural weathering.
- Investigation of adhesive formulations and surface preparation techniques to mitigate stiffness loss in EBR systems.
- Integration of analytical models with predictive numerical simulations to enable parametric studies and design optimization.

By addressing these gaps, future studies can enhance the reliability of composite reinforcement systems and support the transition toward durability-based design in structural engineering.

4.5. Practical implications for design and rehabilitation

The analytical methodology presented in this study provides a practical, efficient tool for evaluating the residual stiffness of composite reinforcement systems subjected to repeated mechanical loading and environmental exposure. Its ability to quantify stiffness degradation in terms of equivalent tensile stress provides engineers with a physically interpretable metric for assessing the long-term performance of reinforced concrete elements.

This capability is particularly valuable in the context of structural rehabilitation and durability-based design. By enabling the comparison of different reinforcement configurations—including EBR, NSM, and hybrid systems—the methodology supports the development and optimization of reinforcement strategies tailored to specific loading and exposure conditions. Engineers can use the approach to identify reinforcement layouts that offer superior long-term performance, thereby improving the reliability and sustainability of strengthened structures.

A key advantage of the proposed model lies in its explicit formulation. Unlike iterative numerical procedures, the model provides closed-form solutions for internal force equilibrium and equivalent stress evaluation. As a result, the analysis's accuracy depends solely on the precision of the experimental measurements, particularly in curvature estimation. This feature makes the methodology well-suited for practical applications, where simplicity, transparency, and reproducibility are essential. The proposed approach bridges the gap between experimental testing and analytical evaluation, offering a robust framework for performance-based assessment of composite reinforcement systems under realistic service conditions. At the same time, the interpretation of the residual stiffness trends reported in this study must be considered within the limitations imposed by the specimen geometry and the analytical model's simplifying assumptions. The slab-like beams were designed to promote smeared cracking and a near-rectangular tensile-stress distribution, ensuring compatibility with the explicit stiffness-evaluation procedure. Consequently, these elements cannot represent the cracking behavior or stiffness evolution of full-scale beams, where crack spacing, bond deterioration, and nonlinear material effects govern the structural response. The equivalent-stress indicator used in this study quantifies the interaction between concrete and reinforcement at the service-load level rather than structural resistance under ultimate or post-yield conditions. Therefore, the long-term stiffness tendencies identified here illustrate material-interaction effects under tightly controlled experimental conditions and should not be interpreted as direct predictors of the structural performance of real-scale reinforced concrete members.

5. Concluding remarks

This study extends a validated analytical model and testing procedure to evaluate the long-term performance of composite reinforcement systems under repeated mechanical loading and environmental exposure. By combining a structured experimental program with a physically grounded analytical framework, the investigation provides practical insights into durability and residual stiffness. Given the limited number of specimens and reinforcement configurations, the findings should be regarded as indicative trends rather than universal design rules. Accordingly, the study demonstrates the applicability and sensitivity of the proposed methodology under realistic service conditions rather than aiming to generalize structural performance at scale.

The interpretation of the reported stiffness trends is conditioned by the analytical framework adopted in this study. All comparisons are performed at the predefined service-load level, ensuring that the equivalent tensile stress reflects the mobilized composite interaction rather than differences in loading magnitude or nonlinear material response. The determined trendline slopes and determination coefficients provide quantitative indicators of whether composite action is preserved or lost under repeated loading and environmental exposure, enabling consistent comparisons across reinforcement configurations. These rules ensure that long-term stiffness tendencies are evaluated under equivalent mechanical demand and are therefore directly comparable across specimen groups and loading histories.

At the same time, the applicability of the reported findings is bounded by the geometry of the bending specimens and the simplifying assumptions of the analytical model. The slab-like beams were intentionally designed to promote smeared cracking and a near-rectangular tensile-stress distribution, ensuring compatibility with the explicit stiffness-evaluation procedure. Therefore, these elements do not replicate the cracking behavior or the evolution of stiffness of full-scale reinforced concrete members, where crack localization, bond deterioration, and nonlinear material effects govern the structural response. The equivalent-stress indicator used in this study quantifies the interaction between concrete and reinforcement at the service-load level rather than structural resistance under ultimate or post-yield conditions. Consequently, the long-term stiffness tendencies identified here reflect material-interaction effects under controlled laboratory and environmental conditions. They should not be interpreted as direct predictors of structural performance in real-scale applications.

5.1. Summary of findings

- The proposed methodology enables quantifying residual flexural stiffness using equivalent tensile stress as a performance indicator.
- NSM reinforcement systems demonstrated superior long-term performance, maintaining higher residual stiffness under both mechanical and environmental stressors.
- EBR systems were more sensitive to environmental exposure, with accelerated stiffness decay observed under open-air conditions.
- Hybrid systems combining steel and EBR reinforcement demonstrated a synergistic effect, reducing vulnerability to environmental degradation even when retrofitted after steel yielding.
- The study revealed the critical influence of residual curvature on stiffness evaluation in retrofitted elements, a factor often overlooked in previous research.

5.2. Methodological contributions

- The proposed methodology provides closed-form solutions for stiffness evaluation, ensuring simplicity and reproducibility for practical durability-based design.
- Using equivalent tensile stress at a consistent service load level enables meaningful and scalable comparisons across reinforcement systems and exposure conditions.

5.3. Recommendations for future research

- Future research must establish standardized protocols for stiffness evaluation under combined mechanical and environmental actions to ensure consistency and reliability in durability assessments.
- Further investigations should rigorously analyze adhesive formulations, surface preparation methods, and environmental conditioning strategies to enhance the long-term bond performance of EBR systems.
- Upcoming studies should broaden the methodology to include other degradation mechanisms—such as chemical attack and creep—and integrate predictive numerical simulations to enable advanced durability-based design optimization.

CRediT authorship contribution statement

Haji Akbar Sultani: Writing – original draft, Visualization, Investigation, Formal analysis, Data curation. **Viktor Gribniak:** Writing – review & editing, Validation, Supervision, Methodology, Conceptualization. **Violetta K. Kytinou:** Software, Resources, Project administration, Data curation. **Aleksandr Sokolov:** Validation, Investigation, Formal analysis.

Declaration of Competing Interest

The authors declare that they have no known competing financial interests or personal relationships that could have influenced the work reported in this paper.

Acknowledgements

Violetta K. Kytinou appreciates the financial support from the Research Council of Lithuania (LMTLT) through the Postdoctoral Scholarship S-PD-24–60.

Data availability

Data will be made available on request.

References

[1] A.T. Obaidat, Flexural behavior of reinforced concrete beam using CFRP hybrid system, Eur. J. Environ. Civ. Eng. 26 (13) (2022) 6165–6187, https://doi.org/10.1080/19648189.2021.1934552.

[2] H.V. Dang, D.N. Phan, Experimental investigation and analysis of pure bending plastic hinge zone in hybrid beams reinforced with high reinforcement ratio under static loads, Eur. J. Environ. Civ. Eng. 26 (13) (2022) 6188–6210, https://doi.org/10.1080/19648189.2021.1934553.
[3] M. Garnevičius, V. Gribniak, Developing a hybrid FRP-concrete composite beam, Sci. Rep. 12 (2022) 16237, https://doi.org/10.1038/s41598-022-20666-x.
[4] H. Zhang, X. Sun, Y. Wang, Bond performance of NSM FRP–concrete interfaces with epoxy under chloride-salt conditioned environments, Struct. Concr. 25 (3) (2024) 2269–2288, https://doi.org/10.1002/suco.202301112.
[5] S.W. Fathuldeen, M.A. Qissab, Behavior of RC beams strengthened with NSM CFRP strips under flexural repeated loading, Struct. Eng. Mech. 70 (1) (2019) 67–80, https://doi.org/10.12989/sem.2019.70.1.067.
[6] H. Shi, J. Guo, Z. Xia, B. Tang, F. Yuan, W. Wang, S. Gu, Detection of interfacial bonding defects in FRP-strengthened concrete using thermal deformation analysis and DIC, Case Stud. Constr. Mater. 23 (2025) e05471, https://doi.org/10.1016/j.cscm.2025.e05471.
[7] M.A. Shayanfar, M. Ghanooni-Bagha, S. Afzali, Reinforced concrete columns strengthened with near-surface mounted and hybrid FRP under compression with or without eccentricity: Experimental study and finite element modeling, Case Stud. Constr. Mater. 20 (2024) e02761, https://doi.org/10.1016/j.cscm.2023.e02761.
[8] V. Gribniak, G. Kaklauskas, L. Torres, A. Daniunas, E. Timinskas, E. Gudonis, Comparative analysis of deformations and tension-stiffening in concrete beams reinforced with GFRP or steel bars and fibers, Composites Part B Engineering 50 (2013) 158–170, https://doi.org/10.1016/j.compositesb.2013.02.003.
[9] A. Rimkus, J.A. Barros, V. Gribniak, M. Rezazadeh, Mechanical behavior of concrete prisms reinforced with steel and GFRP bar systems, Compos. Struct. 220 (2019) 273–288, https://doi.org/10.1016/j.compstruct.2019.03.088.
[10] T. Less, A. Demir, H. Sezen, Structural performance and corrosion resistance of fiber reinforced polymer wrapped steel reinforcing bars, Constr. Build. Mater. 366 (2023) 130176, https://doi.org/10.1016/j.conbuildmat.2022.130176.
[11] V. Gribniak, Material-oriented engineering for eco-optimized structures — A new design approach, Adv. Mater. Lett. 14 (1) (2023) 23011713, https://doi.org/10.5185/amlett.2023.011713.
[12] H.-D. Yun, S.-H. Kim, W. Choi, Determination of mechanical properties of sand-coated carbon fiber reinforced polymer (CFRP) rebar, Polymers 15 (9) (2023) 2186, https://doi.org/10.3390/polym15092186.
[13] A. Wdowiak-Postulak, M. Wieruszewski, F. Bahleda, J. Prokop, J. Brol, Fibre-reinforced polymers and steel for the reinforcement of wooden elements—experimental and numerical analysis, Polymers 15 (9) (2023) 2062, https://doi.org/10.3390/polym15092062.
[14] H.A. Sultani, A. Sokolov, A. Rimkus, V. Gribniak, Quantifying the residual stiffness of concrete beams with polymeric reinforcement under repeated loads, Polymers 15 (16) (2023) 3393, https://doi.org/10.3390/polym15163393.
[15] M. Bazli, A. Jafari, H. Ashrafi, X.-L. Zhao, Y. Bai, R.K. Singh Raman, Effects of UV radiation, moisture and elevated temperature on mechanical properties of GFRP pultruded profiles, Constr. Build. Mater. 231 (2020) 117137, https://doi.org/10.1016/j.conbuildmat.2019.117137.
[16] H. Liu, Q. Jiao, T. Pan, W. Liu, S. Li, X. Zhu, T. Zhang, Aging behavior of biodegradable polylactic acid microplastics accelerated by UV/H_2O_2 processes, Chemosphere 337 (2023) 139360, https://doi.org/10.1016/j.chemosphere.2023.139360.
[17] V. Gribniak, H.A. Sultani, A. Rimkus, R. Boris, A. Sokolov, L. Torres, Quantifying the flexural stiffness changes in the concrete beams with externally bonded carbon fiber sheets under elevated environment temperature, Alex. Eng. J. 104 (2024) 688–700, https://doi.org/10.1016/j.aej.2024.08.044.
[18] A. Dushimimana, J. Sena-Cruz, L. Correia, J.M. Pereira, S. Cabral-Fonseca, R. Cruz, Durability of bond between EBR-CFRP laminate and concrete after four years of natural outdoor and accelerated ageing exposures, Constr. Build. Mater. 427 (2024) 136213, https://doi.org/10.1016/j.conbuildmat.2024.136213.
[19] J.M. de Sena Cruz, J.A. Oliveira de Barros, Bond between near-surface mounted carbon-fiber-reinforced polymer laminate strips and concrete, ASCE J. Compos. Constr. 8 (6) (2004) 519–527, https://doi.org/10.1061/(ASCE)1090-0268(2004)8:6(519).
[20] V. Gribniak, H.A. Sultani, A. Rimkus, A. Sokolov, L. Torres, Standardised quantification of structural efficiency of hybrid reinforcement systems for developing concrete composites, Compos. Struct. 274 (2021) 114357, https://doi.org/10.1016/j.compstruct.2021.114357.
[21] A.M. Araba, O.H. Zinkaah, M. Alhawat, A. Ashour, Experimental tests of two span continuous concrete beams reinforced with hybrid GFRP-steel bars, Structures 47 (2023) 2485–2500, https://doi.org/10.1016/j.istruc.2022.12.055.
[22] K. Xie, Y. Qin, D. Liang, L. Huang, H. Wang, W. Ma, Adjustable arch-beam combination structural strengthening system for reinforced concrete beam bridge, Mech. Adv. Mater. Struct. 30 (18) (2023) 3790–3802, https://doi.org/10.1080/15376494.2022.2083734.
[23] S. Kartal, I. Kalkan, H.C. Mertol, E. Baran, Influence of the proportion of FRP to steel reinforcement on the strength and ductility of hybrid reinforced concrete beams, Eur. J. Environ. Civ. Eng. 27 (12) (2023) 3546–3565, https://doi.org/10.1080/19648189.2022.2143429.
[24] A.A. Abadel, Flexural behaviour of RC beams with a UHPFRC top layer and hybrid reinforcement of steel and glass fiber reinforced polymer bars, Case Stud. Constr. Mater. 21 (2024) e04017, https://doi.org/10.1016/j.cscm.2024.e04017.
[25] N. Khodadadi, H. Roghani, E. Harati, M. Mirdarsoltany, F. De Caso, A. Nanni, Fiber-reinforced polymer (FRP) in concrete: A comprehensive survey, Constr. Build. Mater. 432 (2024) 136634, https://doi.org/10.1016/j.conbuildmat.2024.136634.
[26] S. Afzali, S.A.E. Afzali, M.A. Shayanfar, M. Ghanooni-bagha, M. Afzali, Predictive models for the axial capacity of NSM- and hybrid FRP-strengthened RC columns using ensemble learning optimized by metaheuristic algorithms, Case Stud. Constr. Mater. 23 (2025) e05167, https://doi.org/10.1016/j.cscm.2025.e05167.
[27] R.M. Faysal, M.M.H. Bhuiyan, K.A. Momin, T. Tafsirojjaman, Y. Liu, A review on the advances of the study on FRP-concrete bond under hygrothermal exposure, Constr. Build. Mater. 363 (2023) 129818, https://doi.org/10.1016/j.conbuildmat.2022.129818.
[28] K. Saad, A. Lengyel, Strengthening timber structural members with CFRP and GFRP: A state-of-the-art review, Polymers 14 (12) (2022) 2381, https://doi.org/10.3390/polym14122381.
[29] G.G. Triantafyllou, T.C. Rousakis, A.I. Karabinis, Effect of patch repair and strengthening with EBR and NSM CFRP laminates for RC beams with low, medium and heavy corrosion, Composites Part B Engineering 133 (2018) 101–111, https://doi.org/10.1016/j.compositesb.2017.09.029.
[30] A. Cornejo, S. Jiménez, L.G. Barbu, Numerical analysis of damage in composites: From intra-layer to delamination and data-assisted methods, Mathematics 13 (10) (2025) 1578, https://doi.org/10.3390/math13101578.
[31] G. Ghosh, D. Biswas, R. Bhattacharyya, Advancements in multiscale modeling of damage in composite materials: A comprehensive review, Composites Part B Engineering 307 (2025) 112819, https://doi.org/10.1016/j.compositesb.2025.112819.
[32] S. Mobarhan Zad, M. Rahai, S. Ranjbar, F. Moghadas Nejad, Structural damage analysis using finite element model updating enhanced by response surface methodology, Sci. Rep. (2026), https://doi.org/10.1038/s41598-025-30679-x.
[33] Sultani, H.A., Gribniak, V., Rimkus, A., Sokolov, A., & Torres, L. (2021). Residual stiffness analysis of flexural concrete elements with composite reinforcement. In Proc. of the 13th *fib* International PhD Symposium in Civil Engineering (pp. 94–101). fib: Lausanne. Available at ⟨https://www.fib-international.org/publications/fib-proceedings/13th-phd-symposium-in-paris-france-2020-proceedings-em-pdf-em-detail.html⟩ (visited at 2025-11-10).
[34] F. Soave, L. Ferrara, A durability-based design approach for structural applications with advanced cement-based materials, Case Stud. Constr. Mater. 22 (2025) e04294, https://doi.org/10.1016/j.cscm.2025.e04294.
[35] S. Barbhuiya, B.B. Das, A. Rajput, V. Katare, A.K. Das, Structural performance and implementation challenges of next-generation concrete materials, Structures 81 (2025) 110169, https://doi.org/10.1016/j.istruc.2025.110169.
[36] R.J. Tirado-Gutiérrez, R. González-Drigo, Y.F. Vargas-Alzate, The importance of structural configuration in the seismic performance and reliability of buildings, Infrastructures 10 (12) (2025) 325, https://doi.org/10.3390/infrastructures10120325.
[37] B. Kordtabar, M. Dehestani, O. Yazdanpanah, A. Hasanzadeh, Time dependent seismic fragility and serviceability assessment of reinforced concrete frames under chloride induced corrosion, Sci. Rep. 15 (1) (2025) 40575, https://doi.org/10.1038/s41598-025-24197-z.
[38] Sultani, H.A., Rimkus, A., Sokolov, A., & Gribniak, V. (2022). A new testing procedure to quantify unfavourable environmental effect on mechanical performance of composite reinforcement system. In Proceedings of the 14th *fib* International Ph.D. Symposium in Civil Engineering, 5-7 September 2022, Rome, Italy. *fib*, Lausanne, 2022; pp. 377–384.
[39] V. Gribniak, L. Plioplys, V. Antonovič, A. Sokolov, A. Kudžma, Systematic investigation of the bond performance of steel reinforcement in refractory castables after high-temperature treatment, Constr. Build. Mater. 491 (2025) 142715, https://doi.org/10.1016/j.conbuildmat.2025.142715.

[40] CEN (European Committee for Standardization), Eurocode 2: Design of concrete structures—Part 1-1: General rules and rules for buildings, CEN, Brussels, 2004, p. 225.
[41] V. Gribniak, V. Cervenka, G. Kaklauskas, Deflection prediction of reinforced concrete beams by design codes and computer simulation, Eng. Struct. 56 (2013) 2175–2186, https://doi.org/10.1016/j.engstruct.2013.08.045.
[42] V. Gribniak, A. Rimkus, L. Torres, D. Hui, An experimental study on cracking and deformations of concrete in tension elements reinforced with multiple GFRP bars, Compos. Struct. 201 (2018) 477–485, https://doi.org/10.1016/j.compstruct.2018.06.059.
[43] A. Rimkus, V. Gribniak, Experimental data of deformation and cracking behaviour of concrete ties reinforced with multiple bars, Data Brief. 13 (2017) 223–229, https://doi.org/10.1016/j.dib.2017.05.038.
[44] Mapei (2016). MapeWrap C UNI-AX: Technical Data Sheet. Retrieved November 10, 2025. Available at ⟨https://cdnmedia.mapei.com/docs/librariesprovider22/products-documents/1_mapewrap-cuni-ax_tds_5045ad29ffc8460392b0a822a77f5c07.pdf⟩ (visited at 2025-11-10).
[45] S&P Clever Reinforcement Company (2020). S&P C-Laminate: Carbon Fibre Reinforced Polymer Laminate for Structural Reinforcement. Available at ⟨https://www.sp-reinforcement.eu/en-EU/products/sp-c-laminate⟩ (visited at 2025-11-10).
[46] R. Kliukas, A. Daniunas, V. Gribniak, O. Lukoseviciene, E. Vanagas, A. Patapavicius, Half a century of reinforced concrete electric poles maintenance: Inspection, field-testing, and performance assessment, Struct. Infrastruct. Eng. 14 (9) (2018) 1221–1232, https://doi.org/10.1080/15732479.2017.1402068.
[47] I. Misiūnaitė, A. Rimkus, V. Gribniak, Developing a lightweight hybrid profile concept with a steel shell and polymeric lattice core for optimal mechanical performance, Compos. Struct. 340 (2024) 118169, https://doi.org/10.1016/j.compstruct.2024.118169.
[48] I. Misiūnaitė, A. Rimkus, V. Gribniak, Developing lightweight steel profile and lattice polymeric core composite for structural use, ThinWalled Struct. 206 (2025) 112697, https://doi.org/10.1016/j.tws.2024.112697.
[49] fib (International Federation for Structural Concrete) (2024). fib Model Code for Concrete Structures (2020). Version 1.2. fib: Lausanne, Switzerland, 748 p.
[50] R. Cruz, L. Correia, S. Cabral-Fonseca, J. Sena-Cruz, Durability of bond of EBR CFRP laminates to concrete under real-time field exposure and laboratory accelerated ageing, Constr. Build. Mater. 377 (2023) 131047, https://doi.org/10.1016/j.conbuildmat.2023.131047.
[51] G.B. Wally, F.C. Magalhães, L.C. Pinto da Silva Filho, From prescriptive to performance-based: An overview of international trends in specifying durable concretes, J. Build. Eng. 52 (2022) 104359, https://doi.org/10.1016/j.jobe.2022.104359.
[52] J.D. Ortiz, S.S. Khedmatgozar Dolati, P. Malla, A. Nanni, A. Mehrabi, FRP-reinforced/strengthened concrete: State-of-the-art review on durability and mechanical effects, Materials 16 (5) (2023) 1990, https://doi.org/10.3390/ma16051990.
[53] G.M. Dalfré, G.A. Parsekian, D.C. Ferreira, Degradation of the EBR-CFRP strengthening system applied to reinforced concrete beams exposed to weathering, IBRACON Struct. Mater. J. 14 (2) (2021) e14208, https://doi.org/10.1590/S1983-41952021000200008.
[54] A. Dushimimana, A.P. Vassilopoulos, J. Sena-Cruz, J.M. Pereira, L. Correia, S. Cabral-Fonseca, R. Cruz, Behavior of CFRP composites and epoxy adhesives after long-term exposure to outdoor and laboratory-controlled environments, Constr. Build. Mater. 438 (2024) 137201, https://doi.org/10.1016/j.conbuildmat.2024.137201.
[55] Y. Kusuma, T. Rashmi, V.N. Anand, N. Balaji, An experimental study on flexural performance of RC beams strengthened by NSM technique using GFRP strips for a resilient infrastructure system, Mater. Today. Proc. 52 (2021) 1959–1967, https://doi.org/10.1016/j.matpr.2021.11.600.
[56] W. Van Paepegem, J. Degrieck, A new coupled approach of residual stiffness and strength for fatigue of fibre-reinforced composites, Int. J. Fatigue 24 (7) (2002) 747–762, https://doi.org/10.1016/S0142-1123(01)00194-3.
[57] S.M. Anas, M. Alam, H.F. Isleem, H.M. Najm, M.M.S. Sabri, Ultra high performance concrete and C-FRP tension rebars: A unique combinations of materials for slabs subjected to low-velocity drop impact loading, Front. Mater. 9 (2022) 1061297, https://doi.org/10.3389/fmats.2022.1061297.
[58] A. Metawa, M. Leblouba, S. Barakat, Hybrid reinforced concrete frames with engineering cementitious composites: Experimental and numerical investigations, Sustainability 16 (22) (2024) 10085, https://doi.org/10.3390/su162210085.
[59] T. Ülger, M. Cavuslu, Durability and flexural behavior of concrete-filled hybrid GFRP beams with various interface treatments under humid environmental exposure, Case Stud. Constr. Mater. 23 (2025) e04988, https://doi.org/10.1016/j.cscm.2025.e04988.
[60] X. Wang, Q. Yang, X. Peng, K. Xia, B. Xu, A review of mechanical performance studies on composite concrete beams and slabs, Materials 18 (14) (2025) 3259, https://doi.org/10.3390/ma18143259.
[61] J.A. Olsson, S. Ranganath, S.A. Miller, J.D. Kneifel, A framework for a performance-based sustainability comparison of concrete, J. Clean. Prod. 525 (2025) 146537, https://doi.org/10.1016/j.jclepro.2025.146537.
[62] C.R. Rusnak, Sustainable strategies for concrete infrastructure preservation: A comprehensive review and perspective, Infrastructures 10 (4) (2025) 99, https://doi.org/10.3390/infrastructures10040099.